Hogan, M.T.; Edge, A.C.; Geach, J.E.; Grainge, K.J.B.; Hlavacek-Larrondo, J.; Hovatta, T.; Karim, A.; McNamara, B.R.; Rumsey, C.; Russell, H.R.; Salomé, P.; Aller, H.D.; Aller, M.F.; Benford, D.J.; Fabian, A.C.; Readhead, A.C.S.; Sadler, E.M.; Saunders, R.D.E.

High radio-frequency properties and variability of brightest cluster galaxies

Published in:
Monthly Notices of the Royal Astronomical Society

DOI:
10.1093/mnras/stv1518

Published: 01/01/2015

Document Version
Publisher's PDF, also known as Version of record

Monthly Notices
of the
ROYAL ASTRONOMICAL SOCIETY

MNRAS **453,** 1223–1240 (2015) doi:10.1093/mnras/stv1518

High radio-frequency properties and variability of brightest cluster galaxies

M. T. Hogan,[1,2,3★] A. C. Edge,[1] J. E. Geach,[4] K. J. B. Grainge,[5] J. Hlavacek-Larrondo,[6,7,8] T. Hovatta,[9,10] A. Karim,[11] B. R. McNamara,[2,3] C. Rumsey,[12] H. R. Russell,[13] P. Salomé,[14] H. D. Aller,[15] M. F. Aller,[15] D. J. Benford,[16] A. C. Fabian,[13] A. C. S. Readhead,[9] E. M. Sadler[17] and R. D. E. Saunders[12]

[1]*Centre for Extragalactic Astronomy, Department of Physics, Durham University, Durham DH1 3LE, UK*
[2]*Department of Physics and Astronomy, University of Waterloo, Waterloo, ON N2L 3G1, Canada*
[3]*Perimeter Institute for Theoretical Physics, Waterloo, ON N2L 2Y5, Canada*
[4]*Centre for Astrophysics Research, Science & Technology Research Institute, University of Hertfordshire, Hatfield AL10 9AB, UK*
[5]*Jodrell Bank Centre for Astrophysics, School of Physics and Astronomy, The University of Manchester, Manchester M13 9PL, UK*
[6]*Département de Physique, Université de Montréal, C.P. 6128, Succ. Centre-Ville, Montreal, QC H3C 3J7, Canada*
[7]*Kavli Institute for Particle Astrophysics and Cosmology, Stanford University, 452 Lomita Mall, Stanford, CA 943053, USA*
[8]*Department of Physics, Stanford University, 382 Via Pueblo Mall, Stanford, CA 94305, USA*
[9]*Cahill Center for Astronomy & Astrophysics, California Institute of Technology, 1200 East California Boulevard, Pasadena, CA 91125, USA*
[10]*Aalto University Metsähovi Radio Observatory, Metsähovintie 114, FI-02540 Kylmälä, Finland*
[11]*Argelander-Institute of Astronomy, Bonn University, Auf dem Huegel 71, D-53121 Bonn, Germany*
[12]*Astrophysics Group, Cavendish Laboratory, JJ Thomson Avenue, Cambridge CB3 0HE, UK*
[13]*Institute of Astronomy, Madingley Road, Cambridge CB3 0HA, UK*
[14]*LERMA, Observatoire de Paris, 61 Av. de l'Observatoire, F-75014 Paris, France*
[15]*Department of Astronomy, University of Michigan, 311 West Hall, 1085 South University Avenue, MI 48109-1107, USA*
[16]*Observational Cosmology Lab, Code 665, NASA Goddard Space Flight Center, Greenbelt, MD 20771, USA*
[17]*Sydney Institute for Astronomy, School of Physics, The University of Sydney, NSW 2006, Australia*

Accepted 2015 July 7. Received 2015 May 23; in original form 2014 September 12

ABSTRACT

We consider the high radio-frequency (15–353 GHz) properties and variability of 35 brightest cluster galaxies (BCGs). These are the most core-dominated sources drawn from a parent sample of more than 700 X-ray selected clusters, thus allowing us to relate our results to the general population. We find that ≥6.0 per cent of our parent sample (≥15.1 per cent if only cool-core clusters are considered) contain a radio source at 150 GHz of at least 3 mJy ($\approx 1\times10^{23}$ W Hz^{-1} at our median redshift of $z \approx 0.13$). Furthermore, ≥3.4 per cent of the BCGs in our parent sample contain a peaked component (Gigahertz Peaked Spectrum, GPS) in their spectra that peaks above 2 GHz, increasing to ≥8.5 per cent if only cool-core clusters are considered. We see little evidence for strong variability at 15 GHz on short (week–month) time-scales although we see variations greater than 20 per cent at 150 GHz over six-month time frames for 4 of the 23 sources with multi-epoch observations. Much more prevalent is long-term (year–decade time-scale) variability, with average annual amplitude variations greater than 1 per cent at 15 GHz being commonplace. There is a weak trend towards higher variability as the peak of the GPS-like component occurs at higher frequency. We demonstrate the complexity that is seen in the radio spectra of BCGs and discuss the potentially significant implications of these high-peaking components for Sunyaev–Zel'dovich cluster searches.

Key words: galaxies: active – galaxies: clusters: general – galaxies: jets – radio continuum: galaxies.

1 INTRODUCTION

Energetic feedback from accreting supermassive black holes (SMBH) is now widely accepted to play an integral role in the

★ E-mail: m4hogan@uwaterloo.ca

formation and evolution of Universal structure. Such action is commonly invoked to explain a variety of phenomena such as the high-end curtailment of the galaxy luminosity function (e.g. Benson et al. 2003; Bower et al. 2006; Croton et al. 2006), the $M_{\rm BH}$ versus $M_{\rm bulge}$ correlation (e.g. Magorrian et al. 1998; Silk & Rees 1998) and the symmetry seen in the cosmic histories of both star formation and active galactic nuclei (AGN; e.g. Merloni, Rudnick & Di Matteo 2004; Springel, Di Matteo & Hernquist 2005; Hopkins 2012).

In the most massive systems, at the centres of galaxy clusters, it is now well established that the AGN action of the centrally located brightest cluster galaxy (BCG) prevents runaway cooling (the classical *Cooling Flow Problem*: see Fabian 1994, for a review) by imparting energy to its surroundings through mechanical feedback (see the recent reviews by McNamara & Nulsen 2007, 2012; Fabian 2012). Such actions are invoked to explain the deficit of cold gas (e.g. Edge 2001; Salome & Combes 2003) and star formation (O'Dea et al. 2008; Rafferty, McNamara & Nulsen 2008) compared to what would be expected from cooling dominated systems, as well as the dearth of gas at intermediate cooling temperatures (Peterson et al. 2003). Striking observational evidence for this mechanical feedback is seen through the presence of X-ray cavities in the intracluster medium (e.g. Fabian et al. 2000; McNamara et al. 2000; Hlavacek-Larrondo et al. 2012). These cavities, which are inflated by the actions of co-spatially observed radio-emitting plasma, subsequently redistribute accretion energy from the central SMBH to the surroundings as they buoyantly rise.

There has apparently been a fine balance between heating and cooling within clusters in place for at least half the Hubble time (e.g. Vikhlinin 2006; Pratt et al. 2010; McDonald et al. 2014). Furthermore, the energy imparted by AGN activity does appear to be sufficient to offset cooling *on average* (e.g. McNamara & Nulsen 2007; Dunn & Fabian 2008). However, this is not the case at all times suggesting that periods of cooling must be interspersed by periods of AGN energy injection. Added to this is the growing realization that in the most settled cool-core (CC) clusters where there is a central peak in the cluster X-ray surface profile indicative of substantial cooling, the BCGs have a radio-loud duty cycle approaching unity (e.g. Burns 1990; Mittal et al. 2009; Hogan et al. 2015). This suggests that in these systems there must be cyclic activity whereby the BCG is more active in some periods than others.

Radio observations are integral for tracing this mechanical feedback. However, most studies have been carried out at $\leq$1.4 GHz (e.g. Best et al. 2007) and so the radio properties of BCGs in the $\approx$10–300 GHz range are somewhat poorly constrained. Single-dish surveys of the sky at the higher end of this range are typically shallow with relatively low resolution (e.g. Planck Collaboration XXVIII 2014), whereas even at the lower end, small beam sizes make interferometric surveys of any sizeable area both difficult and expensive. However, several recent surveys have allowed for huge advances in the understanding of the radio sky at greater than 10 GHz (e.g. 10C at 15.7 GHz, Franzen et al. 2011; AT20G at 20 GHz, Murphy et al. 2010 and the AT20-deep (pilot) also at 20 GHz, Massardi et al. 2011; Franzen et al. 2014). Consequently, only a few of the brightest BCGs have well-characterized radio-spectra in this crucial spectral range.

In Hogan et al. (2015; henceforth H15a) we considered the radio properties of BCGs in a parent sample of over 700 X-ray selected clusters comprising the BCS, eBCS and REFLEX cluster catalogues (Ebeling et al. 1998, 2000; Böhringer et al. 2004, respectively). These catalogues are X-ray flux limited, hence our sources are not selected on radio priors and should be representative of the general cluster population. The clusters in the parent sample were split into CCs and non cool-cores (NCCs) using the presence of optical emission lines around the BCG. Such lines are only found in systems with central cooling times less than 5×10^8 years, equivalent to a central entropy less than 30 keV cm^2 and hence can be used as a proxy for the cluster state (Cavagnolo et al. 2008; Rafferty, McNamara & Nulsen 2008; Sanderson, Edge & Smith 2009). The radio spectral energy distributions (SEDs) of the BCG in 246 of these were populated, typically between 74 MHz and 20 GHz, and decomposed into active and inactive components attributable to ongoing and historical accretion, respectively (see H15a). Not only was the radio duty cycle of BCGs in CCs seen to be substantially higher than in NCCs, it was found that the majority of CC-hosted BCGs showed evidence for ongoing core activity that manifests itself primarily as a spectral flattening above a few GHz. Often this emission is missed in low-frequency surveys. Further confounding the lack of information, increased variability is postulated to higher radio frequencies as the emission is expected to originate from increasingly smaller physical scales.

In this paper we select a sub-sample of the BCGs studied in H15a, believed to contain the most active cores. These sources all reside in CC clusters where active feedback is prevalent. Furthermore, the pre-eminence of the radio core component in the radio SEDs of these sources indicates that the SMBH is actively accreting at a significant rate. We have observed them with a variety of facilities to extend their radio coverage up to 353 GHz as well as observing a number of them at different epochs which, alongside historical observations, allows us to study their variability. We reiterate that these sources are from an X-ray selected cluster catalogue. By selecting the sources with the highest expected *core* flux we are able to search for variability via short observations. This permits us to explore the origin of the point-like central radio emission as well as to constrain the amplitude of variation in the accretion rate during active periods of ongoing feedback. Whilst the feedback powers derived from X-ray cavities trace the AGN energy output averaged over tens of megayears, this shorter term variability provides insights into the more instantaneous processes within the core.

One system that has been well monitored at radio frequencies greater than a few GHz, and indeed constitutes one of the most well-studied examples of active AGN feedback in a cluster core, is NGC1275/3C84 in the Perseus Cluster (e.g. Böhringer et al. 1993; Conselice et al. 2001; Abdo et al. 2009). Large amplitude variations in the radio spectrum of this source have been known for many years (Pauliny-Toth & Kellermann 1966).

Recently Dutson et al. (2014) undertook a comprehensive study of the radio and gamma-ray properties of NGC1275, considering its radio variability over five decades in both time and frequency. The radio spectrum consists of a steep spectrum power-law at frequencies below approximately 1 GHz and an inversion above this leading to a peaked profile. It should be noted that the source is not strongly beamed (Krichbaum et al. 1992; Nagai et al. 2010). The power-law component, attributed largely to the presence of extended lobes and a 300-kpc mini-halo (Burns et al. 1992), is constant in its flux. However the peaked component is found to vary significantly in both flux (more than an order of magnitude) and turnover frequency on few year/decade time-scales. Such variations have been previously linked to individual components in the jet on milliarcsecond scales, as recoverable using Very Long Baseline Interferometry (VLBI; e.g. Suzuki et al. 2012). Interestingly, Dutson et al. (2014) find compelling correspondence between this few-year variation of the high radio-frequency peaked component and the high-energy gamma-ray emission but no strong connection between the short-term 'flaring' seen in the gamma-rays and the

1.3 mm flux. In a study of the core X-ray properties of 57 BCGs, Russell et al. (2013) found that roughly half contained an X-ray point source at *Chandra* resolution. It is worth noting that three of these (A2052, Hydra-A and M84) were seen to vary over similar six-month to decade time-scales, similar to the radio emission in NGC1275.

One of the aims of this paper is to investigate whether the high-radio-frequency properties of NGC1275 mark it out as a peculiar object or whether such periods of high activity in the spectral range above 10 GHz are common amongst the BCG population.

Recently the Sunyaev–Zel'dovich (SZ) effect (Sunyaev & Zel'dovich 1972) has been used to compile large catalogues of galaxy clusters (e.g. Vanderlinde et al. 2010; Marriage et al. 2011b; Planck Collaboration VIII 2011a; Hasselfield et al. 2013; Planck Collaboration VII 2013; Reichardt et al. 2013; Planck Collaboration XXIX 2014). Unresolved radio sources present a significant systematic for these searches and may lead to underestimated or completely removed SZ decrement in the 15–200 GHz range (see e.g. Knox, Holder & Church 2004; Coble et al. 2007; Lin et al. 2009). Furthermore, the single-dish nature of many SZ-observatories means that often the removal of contaminating point sources has to rely on uncertain extrapolation of higher resolution but lower frequency data. Our results therefore have potentially significant implications for SZ studies of clusters.

This paper is arranged as follows. In Sections 2 and 3 we describe the sample selection, data collection and reduction. Our results are presented in Section 4 and discussed in Section 5 before we draw conclusions in Section 6. We have used a standard ΛCDM cosmology with $\Omega_{\rm m} = 0.3$, $\Omega_\Lambda = 0.7$ and $H_0 = 70$ km s^{-1} Mpc^{-1}. We use the spectral index convention $S \propto \nu^{-\alpha}$. Unless other stated, we use the name of the parent cluster to refer to its BCG.

2 SAMPLE

The sample of sources chosen for this study were selected primarily from H15a as having the brightest (>10 mJy at 5 GHz), flat-spectrum cores ($\alpha < 0.5$) so a detection above 100 GHz was possible. The H15a sample covers an all-sky, X-ray flux-limited sample of over 700 clusters as outlined above, but the number of sources matching these flux and index cuts is relatively small (<30 or <4 per cent). To increase the target list we added seven bright (>50 mJy at 5 GHz) sources either in fainter clusters and/or clusters misidentified until now. Four of these sources are in fainter clusters (A11, Perlman, Schachter & Stocke 1999; 4C+55.16, Iwasawa et al. 1999; A2270, Healey et al. 2007; and RXJ2341+00) and three in clusters above the eBCS/REFLEX flux limit (RXJ1350+09; RXJ1832+68, Böhringer et al. 2000; Gioia et al. 2003; and E1821+64, Russell et al. 2010). All seven of these sources have been previously identified as AGN, given the association of radio and X-ray emission. However, only E1821+64 is actually strongly (more than 50 per cent) contaminated in the X-ray by an AGN, in this case a quasi-stellar object (QSO). In the other six cases the cluster has *previously* been misidentified as a BL-Lac as a result of them having seemingly flat radio spectra and so the X-rays had been attributed to the AGN. However, all six of these clusters have central galaxies with strong, narrow optical line emission, characteristic of cooling flow BCGs (Crawford et al. 1999) and in all other aspects are similar to the sources selected in H15a. Therefore, we propose a re-identification of each source such that the X-rays are predominantly from the cluster and not a central AGN.

The source selection is by no means complete but is representative of the brightest, core-dominated radio sources in cluster cores. Therefore we believe that the spectral and variability properties we determine for this radio-bright sample can be used to constrain the properties of the complete, X-ray selected sample as a whole.

3 DATA

3.1 GISMO

GISMO is a 150 GHz (2-mm) bolometer camera built by the Goddard Space Flight Centre (Staguhn et al. 2008) for use on the IRAM-30m telescope,[1] which is located at an altitude of 2850 m on Pico Veleta, Spain. GISMO operates as a visitor instrument, being operable for around a two week period every six months. During its time on the telescope GISMO is operated in a shared risk pool observing mode, during which telescope focus and pointing observations are regularly performed on IRAM calibrator sources.

We obtained data from three epochs, using GISMO to observe 29, 24 and 17 sources in 2012 April, November and 2013 April observing runs, respectively, with as many source overlaps between runs as possible (see Table 2; available as online Supporting Information). Sources were typically observed for 5–10 min using a standard lissajous scanning script. The telescope has a full width at half-maximum (FWHM) of 16.7 arcsec and the absolute flux calibration of GISMO is found to have a typical 8 per cent uncertainty.[2]

Data were reduced using the GISMO specific section of the CRUSH software package (Kovács 2008). Pointing and flux models specific to each run are updated during each GISMO run and the package itself is being continually updated. We therefore reduced our data using a version of CRUSH (2.15-2) that post-dates all of our data and hence contains optimized parameters for each of our data sets.

Most of our sources have signal-to-noise ratios (SNRs) less than 10 for each scan. We therefore found the *-faint* option within CRUSH to deliver the best results in most cases. For non-detections we remapped the data using the *-deep* filtering. Only one source (A1885) was recovered using *-deep* but not *-faint*. Since the *-deep* option is known to overfilter sources with SNR greater than 5 and will create negative flux haloes, we took our flux measurements from the maps created using the *-faint* option. A1885 was recovered with a SNR of ≈4 and hence measuring the flux from the *-deep* map for this source is not believed to introduce any additional error. The specific filtering mode used for each source is shown in Table 2. Atmospheric extinction is automatically corrected for within CRUSH, using an estimate of the most recent tau225 GHz value as measured by the on-site tau meter. However, some of our data (particularly during the 2012 November run) suffered from a faulty tau meter not inserting the correct measurement into the FITS file. Time-dependent records of the on-site tau values were recorded manually during each run, which were compared to the values recorded automatically in the log files. To ensure consistency, we manually inputted the best-estimate zenith tau-value using the *-tau.225 GHz* option for each of our source reductions.

Maps were produced and fluxes extracted using the CRUSH tool SHOW. Gaussian fits were performed for each source with the resultant flux and FWHM reported along with source peak and map

[1] IRAM is supported by INSU/CNRS (France), MPG (Germany) and IGN (Spain).

[2] Performance reports available for each run at http://www.iram.es/IRAMES/mainWiki/Continuum/GISMO/Main

RMS in Table 2. Only Hydra-A showed significant extent and hence its flux was extracted from a user-defined region. Fluxes were additionally verified using the KVIS data-display tool (Gooch 1996).

3.2 CARMA

23 sources were observed at 90 GHz using the CARMA interferometer (e.g. Woody et al. 2004) in D-array between 2012 May 21–June 15, of which 20 overlap with our GISMO sources. These observations were performed in queue mode by initiating pre-determined blocks, which could be started and abandoned part way through, depending on observing conditions and at the discretion of the telescope operator. Each block contained an observation of a planet for primary flux calibration. This observation is run through CARMA pipelines to provide a primary flux scale for the observations. Additionally, a strong bandpass calibrator was observed for each block (the bandpass calibrator used was either 3C279, 3C345, 3C454.3 or 3C446, depending on observability). Science targets were visited several times at various hour angles to maximize uv-coverage and sandwiched between 1 min observations of a nearby phase calibrator.

Data were reduced by the standard methods using the CARMA optimized version of the MIRIAD data-reduction software package (developed and maintained by University of Maryland). Some automatic flagging of bad data is performed, but the visibilities were also inspected and flagged interactively. Files with basic calibration, taken at the time of observation, were provided and used as a calibration 'starting point'. Corrections for antenna positions were performed using the most co-temporal *antpos* models provided by the observatory. Further bandpass, phase and flux corrections were applied using standard MIRIAD tasks as determined from the observed calibration sources.

Deconvolution and cleaning of the subsequent maps were also performed using MIRIAD and the KVIS data-display tool used to extract fluxes, verified by additionally extracting fluxes using the AIPS task JMFIT.

3.3 AMI

The Arcminute Microkelvin Imager (AMI; Zwart et al. 2008) is a versatile instrument located at the Mullard Radio Astronomy Observatory (MRAO). Optimized for study of the SZ effect, AMI consists of two interferometer arrays: the Small Array, with 10 3.7-m antennas with baselines of 5–20 m; and the Large Array (LA) with eight 12.8 m antennas with baselines of 18–110 m. These arrays are thus optimized for large (3–10 arcmin) and small (30 arcsec–3 arcmin) scale observations, respectively. This set-up allows study of the large-scale SZ effect with accurate characterization of the contaminating radio source environment. Both arrays measure the I+Q polarization at the central frequency of 16 GHz. Data are taken in six channels, each of width 0.72 GHz, over the range 13.9–18.2 GHz, allowing a local spectral index to be determined for strong sources.

We used the AMI-LA to observe 17 of our sources, with each target visited either two or three times in 2012 (see Table 3; available as online Supporting Information). Observations consisted of 8 min integrations sandwiched between 1-min phase calibrator scans. In the April–June scans sources were themselves used for self-calibration. For the September follow-ups we additionally observed nearby phase calibrator sources. 3C 48 and 3C 286 were observed for use as amplitude calibrators.

Data reduction was performed using the local in-house software REDUCE. Reduction pipelines were used to apply amplitude and phase calibration, flag for telescope errors and Fourier transform to produce frequency channels. Additional flagging for bad data was carried out interactively through visual inspection of the channel data.

Data are written out of REDUCE as uv-FITS files which were read into AIPS for deconvolution and cleaning using IMAGR. Maps were produced for each channel in addition to a single image for the full bandwidth. None of our sources were found to be resolved and so fluxes were extracted using the AIPS task JMFIT and verified using KVIS. We investigated the flux calibration and find a typical 5 per cent uncertainty, which we propagate into in our uncertainties.

3.4 OVRO and UMRAO

Since 2007 the Owens Valley Radio Observatory (OVRO) has been using its 40 m telescope to undertake a 15 GHz monitoring campaign of over 1500 radio sources (mainly blazar Fermi-LAT gamma-ray candidates; see Richards et al. 2011). Five of the sources in our sample have been monitored as part of this OVRO monitoring campaign. An additional 11 BCGs that were identified from this work as having strong high radio-frequency emission, have been included within the dynamic queue since 2013 January, allowing regular (typically every 10 d) observations for these sources (see Table 1).

The OVRO 40 m uses off-axis dual-beam optics and a cryogenic high electron mobility transistor low-noise amplifier with a 15.0 GHz centre frequency and 3 GHz bandwidth. The two sky beams are Dicke switched using the off-source beam as a reference, and the source is alternated between the two beams in an ON–ON fashion to remove atmospheric and ground contamination. A noise level of approximately 3–4 mJy in quadrature with about 2 per cent additional uncertainty, mostly due to pointing errors, is achieved in a 70 s integration period. Calibration is achieved using a temperature-stable diode noise source to remove receiver gain drifts and the flux density scale is derived from observations of 3C 286 assuming the Baars et al. (1977) value of 3.44 Jy at 15.0 GHz. The systematic uncertainty of about 5 per cent in the flux density scale is not included in the error bars. Complete details of the reduction and calibration procedure are found in Richards et al. (2011). We check the pipeline data for, and remove, individual scans whose amplitude is obviously discrepant (of which we find less than 1 per cent) and remove a small minority of points where uncertainties reach more than 40 per cent.

Additionally, one of our sources (4C+55.16) that is included within the OVRO monitoring campaign was also monitored at 15 GHz by the 26 m telescope of the University of Michigan Radio Astronomy Observatory (UMRAO; Aller et al. 1985, 2014). The UMRAO monitoring ran between 1984 October and 2007 June, hence is not ongoing. However the addition of the UMRAO data to the OVRO and AMI data means that for this source we have well-sampled light curves at 15 GHz extending forwards from 1985 to the present.

3.5 SCUBA-2

Observations were made using the SCUBA-2 instrument (Holland et al. 2013) on the James Clerk Maxwell Telescope (JCMT) as part of a poor weather programme (JCMT weather Bands 4 and 5, $\tau_{225\ \mathrm{GHz}} = 0.15$–$0.3$) as part of Canadian and UK projects (M12AC15, M12BC18, M12BU38, M13AC16 and M13AU38) between 2012 February and 2013 July. The observations were made in small map ('CV Daisy') mode with integrations of 30 min each.

The observations were reduced using the standard SMURF package (Jenness et al. 2011; Chapin et al. 2013). We used the standard flux

Table 1. Variability indices for the OVRO data. The mean and median time-scales between observations are given in days, with *N* being the total number of times OVRO observed each source during the considered monitoring period (MJD 54470 to MJD 56750, 2008 January 5 to 2014 April 3). Note that a real V.I. is recovered for RXJ0439 when the full monitoring period is considered but not when only using the restricted time-scale (see also Fig. 5). A much better understanding of the longer-term variability of BCGs is expected to become apparent with continued monitoring.

Source	V.I.	Corresponding per cent	Min. detectable per cent	Mean time-scale	Median time-scale	Mean flux (mJy)	*N*
			Extended time baseline (from MJD 54470)				
RXJ1558	NaN	NaN	5.9	7.5	4.0	195.8	303
RXJ0439	8.0	4.0	4.0	5.8	4.0	131.9	393
AS780	NaN	NaN	10.3	9.0	6.0	130.0	205
A2270	22.0	4.4	4.2	7.0	4.0	308.4	326
RXJ1350	NaN	NaN	6.8	7.1	4.0	201.2	321
			Matched time baseline (from MJD 56320)				
RXJ1558	NaN	NaN	5.5	8.3	5.0	261.1	52
RXJ0439	NaN	NaN	3.8	6.3	5.0	131.5	67
AS780	NaN	NaN	10.5	9.6	5.9	128.9	45
A2270	1.7	2.5	2.5	7.1	5.0	321.9	60
RXJ1350	NaN	NaN	6.3	8.4	5.0	195.5	50
			Added to monitoring list MJD 56320				
4C+55.16	0.48	2.2	2.2	6.8	5.0	1539.2	63
A1348	NaN	NaN	15.9	11.4	7.0	55.2	37
A2052	NaN	NaN	6.4	6.1	4.2	272.5	71
A2055	NaN	NaN	11.8	6.2	4.9	120.1	70
A2390	NaN	NaN	11.9	5.6	4.8	88.5	76
A2415	NaN	NaN	10.6	7.3	5.0	123.1	59
A2627	NaN	NaN	11.3	5.5	4.2	99.4	77
A646	NaN	NaN	14.8	9.1	5.0	58.2	47
RXJ0132	NaN	NaN	9.3	7.2	5.0	155.5	60
RXJ2341	NaN	NaN	7.2	6.6	4.1	156.9	65
Z8276	NaN	NaN	11.6	6.8	4.3	95.3	62

calibration of $FCF_{850} = 527 \pm 26$ Jy beam^{-1} pW^{-1}. The resulting maps reached noise levels of typically 4–8 mJy beam^{-1} (depending on conditions) which was sufficient to detect over half of the sources observed.

4 RESULTS

4.1 Spectral energy distributions

In H15a we performed spectral decompositions for a large number of BCG SEDs, finding that in many cases the spectrum flattens above a few GHz, indicative of these sources containing an underlying strong core component. In this paper we expand the spectral coverage for our sub-sample of 35 of these sources into the mm/sub-mm regime. We indeed see that in many instances these active components extend to high frequency and typically rollover at the highest radio-frequencies, consistent with recently accelerated synchrotron populations.

We performed fits to each of our extended SEDs, using the CURVEFIT program of IDL. Generally our sources could be well fitted with either a power-law (equation A2), Gigahertz Peaked Spectrum (GPS; equation A1; also see Orienti & Dallacasa 2014) like component or a combination of these. Individual SEDs, fitting notes and parameters are presented in Appendix A (available as online Supporting Information). Our SCUBA-2 data were included on the SEDs although excluded from the spectral fits as in several cases it appears to be indicative of an additional albeit poorly constrained component becoming prominent in the mm/sub-mm regime (see Section 5.6). Four example SEDs are shown in Fig. 1.

In some instances, as in RXJ0439+05 (panel a of Fig. 1) the GPS-like component is distinct and inverts the spectrum above a break frequency below which we see a steep spectrum power-law tail to lower frequency. These sources are likely to be undergoing powerful recent activity in their cores. At frequencies below the self-absorption turnover of the core component the spectrum becomes dominated by an underlying steep spectrum power-law component, that may be suggestive of the presence of an amorphous halo of confused emission (Kempner et al. 2004; H15a). In other instances, as shown in E1821+644 and 4C+55.16 (panels b and c of Fig. 1) the integrated spectrum shows only a flattening in the GHz range which may stay flat to high frequencies as in E1821+644 or tail off as in the case of 4C+55.16. That almost all CC-hosted BCGs contain radio-AGN suggests these radio sources are long lived. The variety that we see in their radio spectra suggests that the emitted radio flux is not a constant for any given source. The timing of the most recent period of increased radio emission may then dictate the ratio of high radio-frequency core emission to steeper low-frequency emission from more physically extended regions. Yet other sources, such as MACS0242-21 (panel d, Fig. 1) appear well-fitted by a GPS model with a turnover frequency below 1 GHz. Such sources may be classified as compact steep spectrum objects (CSS, O'Dea 1998). These may be dominated by a single period of older activity where the ejected emission has propagated outwards and expanded, permitting the spectral peak to move towards lower frequency.

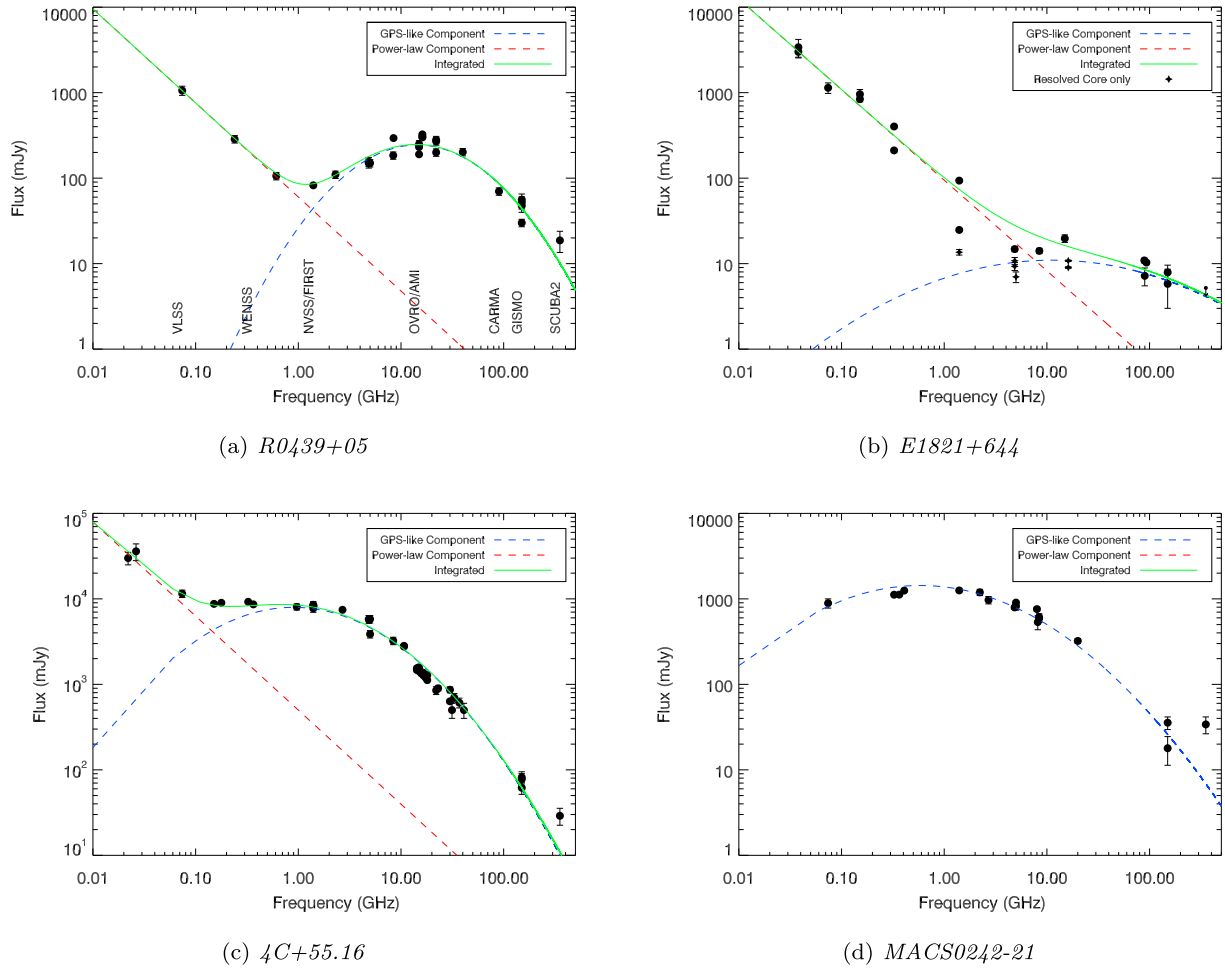

(a) *R0439+05* (b) *E1821+644*

(c) *4C+55.16* (d) *MACS0242-21*

Figure 1. Example SEDs for four objects. In panel (a) we highlight the frequencies of the observations presented within this paper, in addition to the widely used radio-surveys NVSS/FIRST, WENSS and VLSS to help contextualize our frequency coverage. We see a variety of spectral shapes, sometimes well-fitted by a single component as in MACS0242-21 whereas in other cases requiring both a power-law and a GPS-like component (see text). Note that the SCUBA-2 data points at 353 GHz are included in the SEDs but excluded from the plots as they often appear to be suggesting the presence of an additional, poorly constrained component at the highest frequencies (see Section 5.6). [A colour version of this figure is available in the online journal.]

4.1.1 Notes on the general BCG population

26 of the 35 sources are found to contain a GPS-like peaked component. Physically, GPS sources are believed to be young radio sources whose spectra are peaked due to synchrotron self-absorption (O'Dea 1998). That we find peaked components within our BCG spectra, in addition to steep components at low frequency, is indicative of recently enhanced radio emission in the central regions of these objects. This could be associated with a long-lived source having a varying accretion rate, or with the launching of distinct knots in the radio jets. Either scenario is consistent with the high duty cycle expected for these CC-hosted AGN. We plot in Fig. 2 both the peak flux of the fitted GPS component and the combined power-law + GPS-component flux of each of our GPS-containing sources as a function of the GPS turnover frequency. These are mainly found to be GPS dominated at the frequency of the peak, with only a minority of sources found where the combined flux is significantly greater than the GPS component alone.

We find that the spectral turnover of the GPS component in 19 of these 26 sources lies above 2 GHz. Only Hydra-A has a sub-dominant core at the frequency of the core's spectral peak. The presence of the core here therefore does not overtly affect the integrated spectral shape in Hydra-A at frequencies greater than a few GHz. In the simplest case we can use this to put a limit on the number of BCGs containing powerful peaked cores that greatly affect the spectrum above the observing frequency of most wide-sky surveys (e.g. NVSS/FIRST at 1.4 GHz, WENSS/WISH at 325 MHz, VLSS at 74 MHz; see Appendix A; Rengelink et al. 1997; White et al. 1997; Condon et al. 1998; De Breuck et al. 2002; Cohen et al. 2007). Our sample was drawn from the 726-source parent sample of H15a. If we subtract from this the 196 sources that fall below declination -30° and so were not considered by our initial GISMO selection criteria (see Section 2) then we find that $\geq$3.4 per cent of BCGs contain a synchrotron self-absorbed active core component peaking above 2 GHz that is brighter than 10 mJy at *C* band ($\approx$5 GHz). This fraction increases to $\geq$8.5 per cent if we consider only the CC clusters. Our incomplete spectral coverage of the full sample means that this number is only a lower limit and that the true fraction of BCGs with GPS cores may be much higher. Indeed this simple analysis neglects systems whose spectra appear to be persistently flat out to high radio frequencies where multiple superposed flux components may be present.

That strong spectral deviations at frequencies higher than a few GHz are not uncommon in BCGs has important implications. This

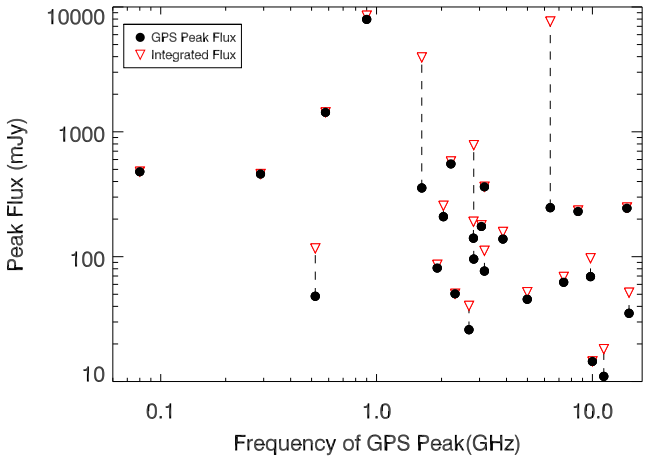

Figure 2. Flux of the GPS-like component as a function of the frequency at the peak. Note that in the classification scheme of O'Dea et al. (1998), the lowest peaking of these components, an isolated source would likely be identified as CSS rather than GPS. However, we note that in the evolution scenario for this family of sources, CSS sources are just slightly older GPS sources and hence we refer to all of these peaked components as 'GPS-like' for brevity. Each source is represented twice (connected by dashed lines). Circles show the peak flux of the GPS component whereas down-facing triangles show the combined flux of both the GPS and any power-law component measured at the GPS turnover frequency. In the majority of instances we see that at the turnover frequency the GPS component is dominating the flux. It should be noted that *virtually all* radio-loud BCGs *may* contain a peaked active component, although in most systems these would be expected to peak far below the integrated flux and hence be undetectable in all but the brightest systems.

includes, but is not limited to, the activity of the population as a whole and also the expected contamination rate of high-frequency peaking radio components in BCGs on SZ signals. We consider this further in Section 5.

4.2 Nature of variability

Understanding the radio variability of AGN is important as it informs us on several physical processes. Short-term variation allows us to place size constraints on the region from where any observed radio flux propagates (i.e. a source cannot vary on less than its crossing time) whereas longer term (few year) variation can inform us as to the likely fuelling mechanisms of AGN. At radio frequencies, the variation itself can be due to differing energy densities within the jet, which may be due to a change in the accretion structure and fuelling rate at the jet base. Alternatively, changes in flux may be due to individual components within a jet becoming brighter as they interact with other material. However, fully characterizing the radio variability of AGN is inherently difficult as the measured variability can be attributed to different mechanisms and will be most prevalent on different time-scales depending on the observing frequency.

As an example, consider a synchrotron self-absorbed source sampled at a frequency just below the turnover which shows a flux increase. Without contemporary observations at and above the peak it would be difficult to say whether the additional received flux is due to an increase in total power-input to the jet by the AGN (and hence the normalization of the entire SED should increase) or whether the overall power output is falling but that the lower intensity and expanded physical scales of the emitting regions lead to the turnover moving to lower frequency and so giving a flux increase below the peak while the overall normalization remains constant. Ideally the entire SED would be sampled simultaneously and fitted, accounting for self-absorption at a variety of epochs in order to recover the true variability in the underlying power output. Unfortunately, such a campaign is prohibitively expensive. Nevertheless, limits can be placed on the variability of BCGs at different frequencies and time-scales.

4.3 Monochromatic variability

4.3.1 Variability index

We use the debiased variability equation (e.g. Akritas & Bershady 1996; Barvainis et al. 2005; Sadler et al. 2006) to attempt to place quantitative limits on the monochromatic flux variability of our sources. This index accounts for the uncertainties in flux measurements and hence should be robust against artificial positives. The variability index (V.I.) is defined as

$$V_{\rm RMS} = \frac{100}{\langle S \rangle} \sqrt{\frac{\sum (S_i - \langle S \rangle)^2 - \sum \sigma_i^2}{N}}, \quad (1)$$

where S_i is an individual flux measurement, σ_i the associated uncertainty, $\langle S \rangle$ the mean flux and N the number of observations of a given source. For light curves with a large number of points this statistic gives a measure of the typical variability of a source about its mean flux. This analysis begins to falter for light curves with a small number of points where the mean is not necessarily representative of all measured fluxes. However, it is useful even in the limit of $N = 2$ as a positive returned V.I. is indicative of significant variation whereas an imaginary returned V.I. suggests any observed flux difference is most likely attributable to measurement uncertainty. A limitation of this method is that overestimation of the error on flux measurements can mask real variability. However, this variability would be below any limits found for variation below the given errors. Given limits on variability would therefore be correct, albeit less restrictive than if less conservative flux uncertainties were used. Although it should be noted that such a limit does not of course restrict the potential for the source to vary below this level. Similarly, underestimation of errors can falsely indicate variability where there is none.

4.3.2 Variability at 15 GHz: OVRO

For the 11 sources added to the OVRO monitoring campaign circa MJD 56320 (2013 January; see bottom panel, Table 1) we find that no sources have a positive V.I. This suggests that for all 11 sources the difference in measured flux is within the 1σ uncertainties of the individual measurements such that this leads to an imaginary value for the square root. This is somewhat surprising, since for a non-varying population we might expect around half to have slightly positive V.I.s and half slightly negative V.I.s. The lack of any positive V.I.s indicates that our flux uncertainties are overestimated. A positive V.I. requires that the numerator within the root of equation (1) be positive, which at the most basic level just requires that the average fractional flux deviation from the mean flux be larger than the mean fractional error.

In Fig. 3 we plot the typical percentage deviation from the mean flux for each source, as well as the mean fractional error on the flux (displayed as a percentage). Additional data are provided in Table 1. We see that in all instances of the 11 sources monitored since 2013 January the typical flux deviation is less than the typical error, hence showing why no real V.I.s were returned. For a non-intrinsically-varying population of sources we might expect ≈68 per cent of flux

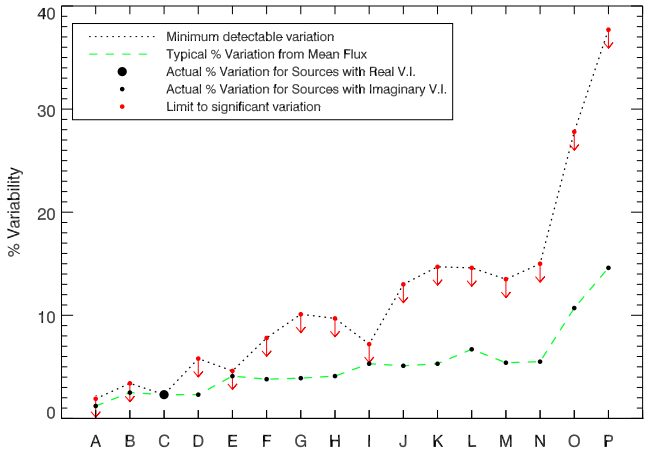

Figure 3. Dotted line shows the minimum percentage variabilities that would have corresponded to a positive V.I. (typical deviation from mean flux greater than mean fractional error) for the OVRO sources, sampled at 15 GHz on typically one-week time-scales. The green dashed line shows the actual typical deviation from the mean flux for each source, respectively. Note that only A2270 shows significant variation (dashed line above dotted line). Sources are arranged left to right by their maximal measured flux at 15 GHz. The detectable percentage variation is typically much lower for brighter sources, with some deviation from a one-to-one correlation due to uncertainties on flux measurements varying by source. Sources are as follows: (A) 4C+55.16, (B) RXJ0439*, (C) A2270*, (D) A2052, (E) RXJ1558*, (F) RXJ2341, (G) RXJ0132, (H) AS780*, (I) RXJ1350*, (J) A2055, (K) A2415, (L) Z8276, (M) A2627, (N) A2390, (O) A646 and (P) A1348. Note that five of these (indicated with *) were in the initial OVRO monitoring list and hence longer time-baseline data are available, where plotted values are those calculated when the time frame was matched to the other 11. See also Table 1.

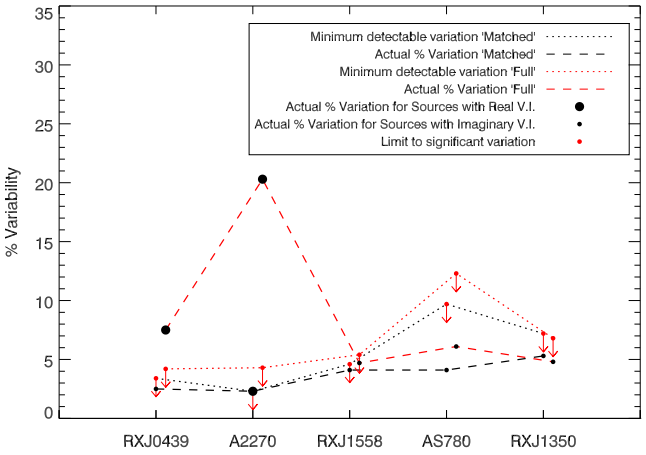

Figure 4. OVRO variabilities for only the five sources in the original lists, measured for the full (from 2008 January onwards, red lines and offset for clarity) and restricted (2013 January onwards, black lines) time frames. Dotted lines show the minimum percentage variabilities that would have corresponded to a positive V.I. (typical deviation from mean flux greater than mean fractional error), whereas dashed lines show the actual typical deviation from the mean flux for each source, respectively. Note that only A2270 shows low-level significant variation (dashed line above dotted line) when only using data during the matched time period whereas when using the full data, both A2270 and RXJ0439 show significant variability, as would be expected by considering the light curves in Fig. 5. Although not a perfect measure, this does show evidence that variability at 15 GHz is most prominent over longer time frames; hence considering variation of BCGs on longer than single year time-scales is important. As in Fig. 3 we order the sources left to right by their maximal measured flux at 15 GHz. See also Table 1. [A colour version of this figure is available in the online journal.]

measurements to lie within one standard error of the mean. That our typical percentage uncertainties are around twice our typical flux deviation from the mean suggests that our errors are overestimated by a factor of 2–3. We cannot steadfastly claim that our sources are intrinsically non-varying and should therefore adhere to Gaussian statistics; hence we merely claim that they typically are restricted to varying by $\leq$10 per cent on roughly one-week time-scales. However, we note that this limit may be a factor of 2–3 lower.

Two of the five sources that were in the OVRO monitoring campaign over the full period (top and middle panels, Table 1) return real variability indices when the V.I. is calculated over the full time range (A2270 and RXJ0439) but only one (A2270) is recovered when the V.I. is calculated over a time range restricted to match that of the other 11 sources (see Fig. 4). In Fig. 5 we show the 15 GHz light curves for these five sources. Clearly both A2270 and RXJ0439 display large flux increases over the full time-scales considered. It is interesting to then note that the variability of RXJ0439 as shown by the increase from MJD 54500–55500 would be missed if considering only the restricted time-scale. This highlights a shortcoming of the V.I. technique. If a source varies significantly (e.g. RXJ0439, Fig. 5, MJD 54500–55500) then its average flux difference from the mean will be much larger than the mean flux and so a positive V.I. will be returned. If the source then continues to be monitored but does not subsequently vary much (e.g. RXJ0439, MJD 55500–57000) then the *average* flux difference from the mean will drop significantly. If data from monitoring over a substantially long time is combined, this will eventually result in the average difference from the mean dropping below the average error and so the measured V.I. is no longer truly reflective of the variability seen early on. The inverse of this effect can be seen by considering A2270 in Figs 4 and 5. A2270's light curve shows that it varies significantly. However, when only the matched time-frame data is used, A2270 returns a barely significant variability (Fig. 3). Conversely, when the longer-term monitoring is included then a very high level of variability is seen (Fig. 4), which better reflects what is evident from its light curve. These effects suggest that at 15 GHz, variability of sources is most likely to be seen in campaigns with high cadence over several year monitoring time-scales.

The measurable percentage variation that would have returned a real V.I. (and therefore a significant measure of variability above the noise) varies from source to source, typically being lower for brighter objects. However, by inspection of Fig. 3, we can claim that the 15 GHz variability of these BCGs is typically restricted to $\leq$10 per cent on roughly one-week time-scales (see Table 1). Additionally, we see evidence that much larger magnitude variation may be common in BCGs on few-year time-scales. This mirrors the finding of Hovatta et al. (2007) who found variability on few-year time-scales in a sample of blazars from a greater than 25-yr monitoring campaign with the UMRAO and Metsähovi telescopes. The OVRO monitoring campaign is ongoing hence the statistics on this longer-term variability will naturally improve with time.

4.3.3 Variability at 150 GHz: GISMO

Of the 35 individual sources observed with GISMO, 23 had at least one repeat observation hence allowing variability to be measured. Of these, and considering only detections, 7 sources were observed at all three epochs with the remaining 16 observed twice. Only four sources returned real two-point Variability Indices, namely

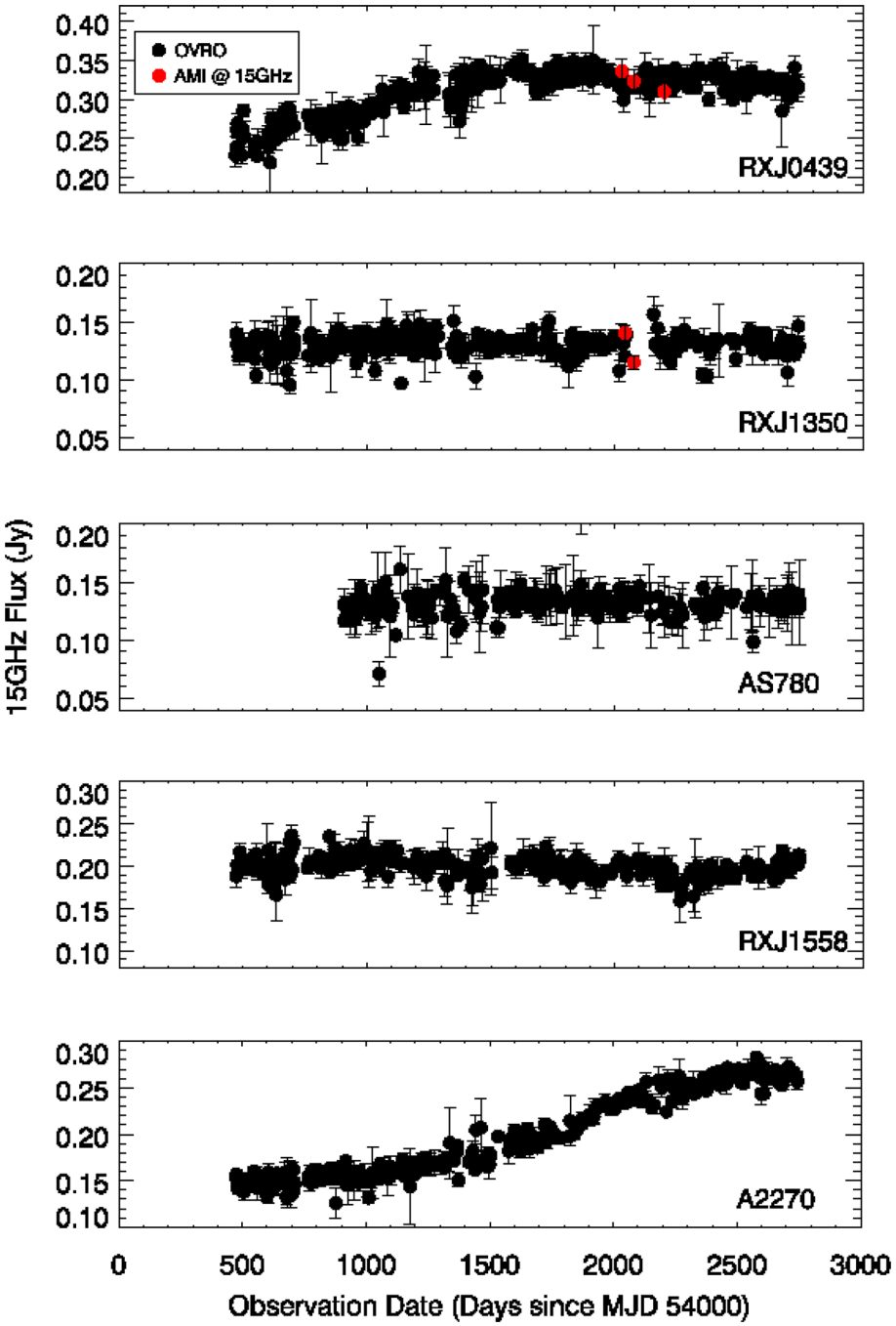

Figure 5. Longer term light curves for the five sources that were in the original list of OVRO targets. Where AMI observations were available, the flux is corrected to 15 GHz using an index fitted to the AMI data split over the six channels for that observation specifically. We see strong variation over typically year time-scales in both RXJ0439 and A2270 at 15 GHz. Note that MJD 54000 corresponds to 2006 September 22.

Z8276 (V.I.=43.5 : 2 observations), A2270 (8.2 : 3), MACS0242 (23.2 : 2) and RXJ1558 (10.2 : 3).

However it should be noted that working out the V.I. for our GISMO-observed sources is less informative than for those observed with OVRO since the V.I. works primarily by determining the difference from the mean flux. Clearly, when only two (or three) observations of a source are available then such an average is less meaningful due to the large uncertainties on the flux. Nonetheless, a real V.I. still indicates which sources are really variable at the investigated cadence. Therefore instead of calculating the minimum detectable typical percentage variation about the mean (as was done for the OVRO data, see Fig. 3), for GISMO we instead calculate the following:

(i) for sources with two observations – the *actual* minimum required percentage change between the first and second fluxes to return a real V.I. (assuming the reported uncertainties);

(ii) for sources with three observations – the *total* minimum required percentage change across three epochs, from the first measured flux assuming a simple model where the observations are symmetrically distributed around the flux of the central observation (i.e. $S_1 - S_2 = S_2 - S_3$). This is a simplistic approach

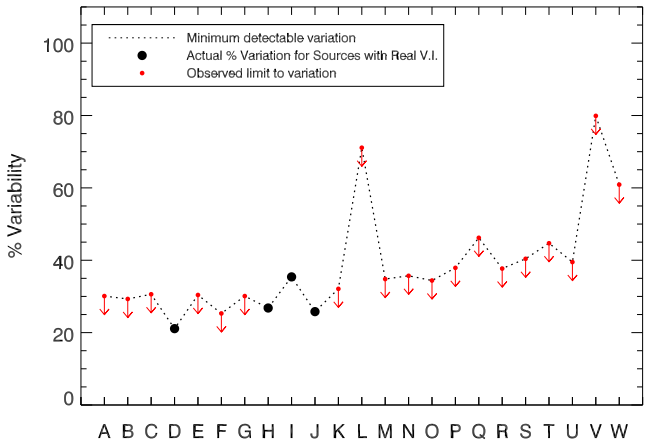

Figure 6. Detectable variabilities that would have corresponded to a positive V.I. for the GISMO sources, sampled at 150 GHz on approximately six-month time-scales. Sources are arranged left to right by their maximal measured flux at 150 GHz. The detectable percentage variation is typically much lower for brighter sources, with some deviation from a one-to-one correlation due to uncertainties on flux measurements varying by source. Sources are as follows: (A) Hydra-A, (B) 4C+55.16, (C) A3581, (D) A2270, (E) RXJ0439, (F) RXJ2341, (G) A2052, (H) RXJ1558, (I) MACS0242, (J) Z8276, (K) A2415, (L) RXJ0132, (M) AS780, (N) A2627, (O) RXJ1350, (P) A2055, (Q) Z8193, (R) A646, (S) RXJ1832, (T) A2390, (U) A496, (V) E1821, (W) PKS0745.

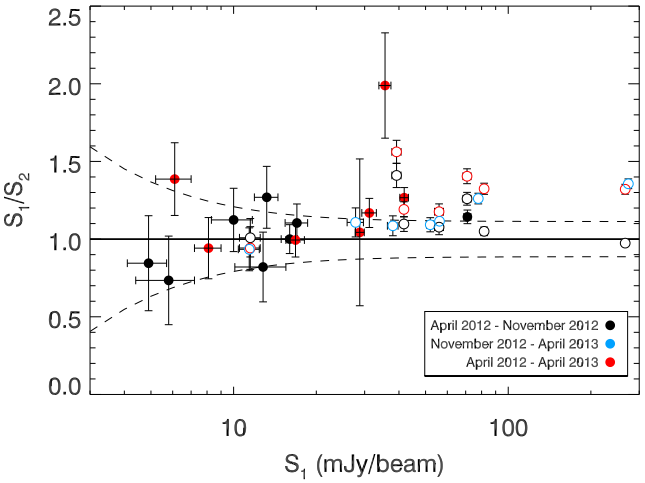

Figure 7. Ratio of the measured GISMO fluxes at 150 GHz between each pair of epochs. The dashed lines indicate the error envelope due to the 8 per cent typical flux uncertainty. Open symbols are for sources that appear more than once due to being observed during all three epochs; consult also Table 2. Sources typically appear to be fading, as expected for a sample chosen as the brightest at the selection epoch. The source that appears to show very strong variation is Z8276, which is seen to fade drastically at 150 GHz between 2012 April and 2013 April.

and would require a source that does not vary between epochs 1 and 2 to vary by twice the expected mean between epochs 2 and 3 to be detected, however it does allow an *estimate* of the minimum average variation per six-month window that would be detectable.

The results of this are plotted in Fig. 6. We see that we are sensitive only to variation of above typically 30 per cent. The *actual* percentage variations of the four sources with real V.I. values are also shown.

In Fig. 7 we plot the fractional flux changes between each pair of GISMO observations for a source. As in Fig. 6 we see that the majority of observed variability is within the error envelope. The large variations of some sources as seen in Fig. 6 are again apparent. One point that becomes obvious in this particular representation is that the majority of our observed variation is of sources fading over the 1–2 years covered. This may hint towards systematic flux offsets between GISMO runs. However, these are carefully checked for[3] and should not dominate. A natural alternative explanation arises simply because we selected the sources to be (likely) the brightest amongst our parent sample at 150 GHz as a result of their lower frequency spectral shapes. These most active sources are therefore likely to have been selected at their peak brightnesses and subsequent follow-ups will naturally be expected to see the flux falling.

The 2013 April observation of M0242-21 was observed with a high optical extinction (tau = 0.70), which may contribute to the GISMO flux drop of about 50 per cent. However, we note that this source is a Submillimeter Array calibrator and shows a similar percentage flux decrease over this period (at 1.3 mm[4]) suggesting that the variability is real.

[3] Performance reports available for each run at http://www.iram.es/IRAMES/mainWiki/Continuum/GISMO/Main

[4] http://sma1.sma.hawaii.edu/callist/callist.html

Given the high error envelopes, that we detect variability amongst our sample of repeat observations at 150 GHz suggests that significant variation of such sources at high radio frequencies may be relatively commonplace over six-month to year time-scales. Such variability has important implications particularly for SZ observations (see Section 5).

4.4 Measuring percentage variation

In addition to a V.I., we also determined a measure of the typical annual absolute percentage variability of the sources monitored by OVRO at 15 GHz. Measuring the maximal percentage variation of a source over any given time period is highly susceptible to measurement uncertainty, since one bad unidentified outlying flux can greatly skew the result. Instead we effectively determine a robust measure of the maximal gradient of the light curve during the monitored period. To do this, we measure the mean of the six percentage differences between the 95th and 5th, 94th and 6th, 93rd and 7th, 92nd and 8th, 91st and 9th and 90th and 10th percentiles (n.b. for sources only in the monitoring list since 2013 January with less than 100 observations, we used the 5th–95th percentile range and the five unique ranges below this to a minimum separation of the 85th and 15th percentiles – beyond this we automatically classified any resulting measured variability as an upper limit).

A mean over six ranges was found, by trial and error, to be a reasonable compromise between too few measurements being susceptible to random fluctuations but too many requiring the inclusion of less-separated percentile differences, over which less variation is expected even for varying sources. We found that taking the 5th–95th percentile range as our maximum ensured that our measurements were robust against outlying data points. Additionally, averaging over an even number of percentile ranges allows non-varying sources to have variations averaging to effectively zero (note that in practice the probability of it *actually* averaging to precisely zero is minimal, however the probability of it approaching zero is increased with an even number).

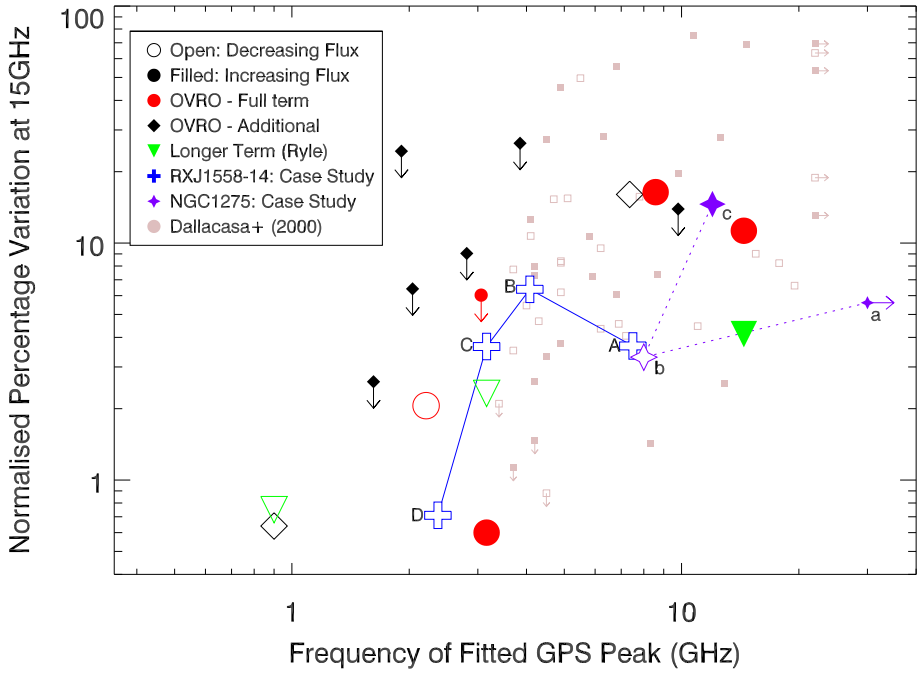

Figure 8. Percentage variation at 15 GHz as a function of the position of the fitted GPS peak. Note that the percentage variation has been normalized to the implied *annual* variation. This allows comparison of sources monitored over different time-scales and with a variety of sampling time-scales. Values for OVRO sources correspond to those calculated in Section 4.4. Three sources have historical observations from the 1970s/80s at 15 GHz with the Ryle telescope (see text, Section 4.4) and we include the percentage variations over these longer time frames, calculated in a similar way for comparison. Open symbols denote flux decreases over the monitored period whereas filled symbols denote flux increases. We see a general tendency for higher peaking sources to be more variable although this is not a strong trend and the ratio is highly dynamic, as highlighted by the case studies of RXJ1558-14 (shown as large crosses) and NGC1275 (shown as large stars – also see Section 5). For comparison we plot as faded points the normalized percentage variations in the OVRO monitoring for the HFP sample of Dallacasa et al. (2000). These inhabit a similar distribution to the peaked components within our BCGs showing that their behaviour is not dissimilar to young radio sources elsewhere. [A colour version of this figure is available in the online journal.]

To determine whether these measured percentage variations most reliably constitute genuine variability or an upper limit on variability, we took a measure of the two-point V.I. values for each of these six percentile ranges. We required that a minimum of four of these return real V.I. values for a value to be assigned to the percentage variation, otherwise the measured percentage variation was taken to be an upper limit. We normalize our mean measured percentage variation values by the mean difference in years between the measurements used, thus recovering a measure of typical annual variation. Where only a limit on variation is recovered, we normalize by the total monitored period in years (roughly 1 yr for the 11 sources added to OVRO list in 2013 January).

Three sources (4C+55.16, RXJ0439+05 and Z8193) have historical 15 GHz data preceding OVRO monitoring from either the UMRAO campaign or pointed observations with the Ryle Telescope. We combine these with the OVRO data and find the percentage variations over longer time-scales.

In Fig. 8 we show our calculated absolute percentage variations at 15 GHz as a function of the peak position of the fitted GPS. A mixture of sources increasing and decreasing in brightness is seen. A weak general trend for the highest peaking sources to show most variability is seen. Such a trend is expected, as a higher turnover frequency suggests self-absorption closer to the jet base and hence emission from smaller scales, which can more easily translate to faster emitted variability. However, it must be noted that the GPS-peak frequency is expected to move and also the variability is non-constant, hence both parameters are expected to undergo linked evolution. We illustrate this dynamic relationship by including on Fig. 8 evolutionary tracks for two sources with long-term monitoring; RXJ1558-14 and NGC1275. Both are seen to move extensively across Fig. 8 but always remain within the region occupied by the other points. We consider these sources as case studies in Sections 5.2 and 5.3.

For comparison with the more general galaxy population we additionally include on Fig. 8 the normalized percentage variations at 15 GHz for the 50 sources (of 56) in the high frequency peaker (HFP) sample of Dallacasa et al. (2000) that are in the OVRO monitoring list. These show a similar weak trend to the peaked components of our BCG spectra, suggesting that our peaked components show similar behaviour to young recently activated sources. This indicates that they are associated with recent episodes of enhanced radio emission.

4.4.1 A GPS link to variability?

The behaviour of NGC1275 and RXJ1558-14 suggest that a direct link between GPS-peak frequency and variability is not present. Instead a dynamic ratio is seen between these parameters whereby the position (and indeed presence) of a self-absorption peak in relation to the observed frequency of a source can have a large effect on the amount of variability seen.

The position of the peak appears to weakly correspond to how quickly a source can vary at a given frequency although not necessarily how quickly it does vary over any given epoch. Indeed, whilst the presence of a flat or peaked component in a BCG's SED can be indicative of it being more likely to vary at high radio

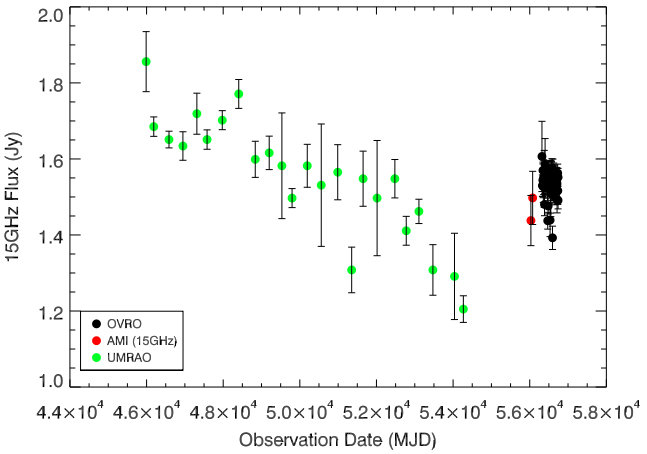

Figure 9. Light curve for 4C+55.16. UMRAO points are the yearly average. Note that AMI observations have a central useable frequency of 16.05 GHz, which was corrected to the value shown here using the in-band spectral index. Note that MJD 46000 corresponds to 1984 October 27.

frequencies there does not appear to be a single observable proxy for the level of variation. The only way to robustly remove high-frequency contaminants remains contemporaneous observation.

It should be noted that GPS sources actually constitute a range of types and that many sources classified in the literature as GPS and HFPs are actually flaring flat spectrum quasars or blazars (see Discussion by Torniainen et al. 2007). The variability of these sources is naturally expected to be different to genuine, long-term GPS objects. Amongst genuine GPS sources the peaked spectral shape is maintained over decade time-scales and long-term variation of the absolute flux level of this is seen (Aller et al. 2002). This longer term variation (years to decades) is similar to what we see in the peaked components of NGC1275 and RXJ1558-14 and hence further supports that the variability herein is likely due to similar physical processes to that in more typical GPS objects, which may be related to opacities within the jet flow.

5 DISCUSSION

5.1 Case study: 4C+55.16

As mentioned in Section 3.4 one of our sources, 4C+55.16, has near-continuous 15 GHz light curves available for almost two decades, allowing us to consider its longer term activity. In Fig. 9 we show the combined light curve consisting of UMRAO, AMI and OVRO observations. Note that our AMI observations have a central frequency of 16 GHz. We fit a single spectral index to the SED of 4C+55.16 above 10 GHz, recovering an index of 1.29[5] and use this to correct our AMI fluxes to 15 GHz.

A steady decline in total flux density is seen towards the end of the UMRAO light curve for this source (2007, MJD $\approx$ 54000). Our AMI fluxes are consistent with those recovered with OVRO, within the errors. However, if we remove the absolute flux calibration of the AMI observations then they are perhaps self-consistent with having caught the source as it brightens, before it is then reasonably steady throughout the OVRO monitoring. Variability of this at 15 GHz is slow, varying by approximately 20 per cent on decade time-scales. This compares to significantly less variability on typically one-week time-scales. However, from the GISMO observations of this source we do get faster variation at higher frequencies showing that although the overall SED may only vary slowly over several years, short-term 'flickering' of the flux at frequencies above 100 GHz is still evident over much shorter periods.

5.2 Case study: RXJ1558-14

RXJ1558-14 shows remarkably similar behaviour to NGC1275, albeit displaying around an order of magnitude less flux. NGC1275 is a well-studied source which constitutes the prototypical example of a variable BCG with a GPS-like component showing steady mm-variability over few year time-scales (see Dutson et al. 2014, for a thorough discussion of the variability properties of NGC1275).

RXJ1558-14 has been monitored by OVRO since 2008 and shows little variation at 15 GHz over this time frame. However, the source has historically been used as both a Very Large Array (VLA) and Very Long Baseline Array (VLBA) phase calibrator and has a wealth of observations available in the National Radio Astronomy Observatory (NRAO) archive. We can therefore study its behaviour over long timelines.

In the top panel of Fig. 10 we show long-term light curves at both *X* band (8.4 GHz) and *C* band (4.8 GHz) for RXJ1558-14, as well as the more recent *U* band (14.9 GHz) monitoring. Data were compiled from the literature and by downloading FITS images for all available observations in the NRAO archive and extracting flux measurements using IMFIT. We split the light curves into four time-windows, indicated on Fig. 10 as 'A', 'B', 'C' and 'D'. In panel A (see Wright & Otrupcek 1990) we see that the 5–8 GHz spectrum was inverted,[6] although this is not the case at later times.

In the middle panel we plot the SED for RXJ1558-14 with data points coded to correspond to these four time-windows. In the bottom panel we focus only on the GPS-like part of the spectrum, again coding the data points although here we additionally show illustrative GPS models to the data in each of the time windows. As we move through time windows A to D we see the GPS peak appear to move both downwards in flux and also in turnover frequency.

RXJ1558-14 displays double-lobed structure on parsec scales with an unresolved central core, as seen at 2.224 and 8.154 GHz in 1997 by Fey & Charlot (2000) and more recently at 4.86 GHz in 2012 (see Hogan et al., in preparation). Although these observations are at different frequencies and thus cannot be used to get any secure measure on the expansion, it is worth noting that no new features are seen to arise between these observations. The lobes seen in the 4.86 GHz map of Hogan et al. (in preparation) lie approximately equidistantly 7 mas either side of the central component. If we associate the high core fluxes observed in 1972 with the launching of these knots then in the intervening 40 yr the knots travel with an apparent transverse velocity of approximately 1.02*c*, permitting viewing angles between 45° and 90° that are entirely consistent with the symmetry seen in the source. It is therefore consistent, and indeed highly likely, that the very high core fluxes observed in the 1970s were attributable to the emission of the features which are now observed as expanding lobes on milliarcsecond scales and the subsequent fall in flux is attributable to these lobes propagating away from the core. Such a scenario would suggest that variability of RXJ1558-14 (and indeed other sources) above a few GHz may

[5] $S = A\nu^{-\alpha}$.

[6] We use 'inverted' within this paper to refer to radio spectra with increasing flux to higher frequency, which is the opposite to the usual scenario for a typical, unobscured synchrotron spectrum.

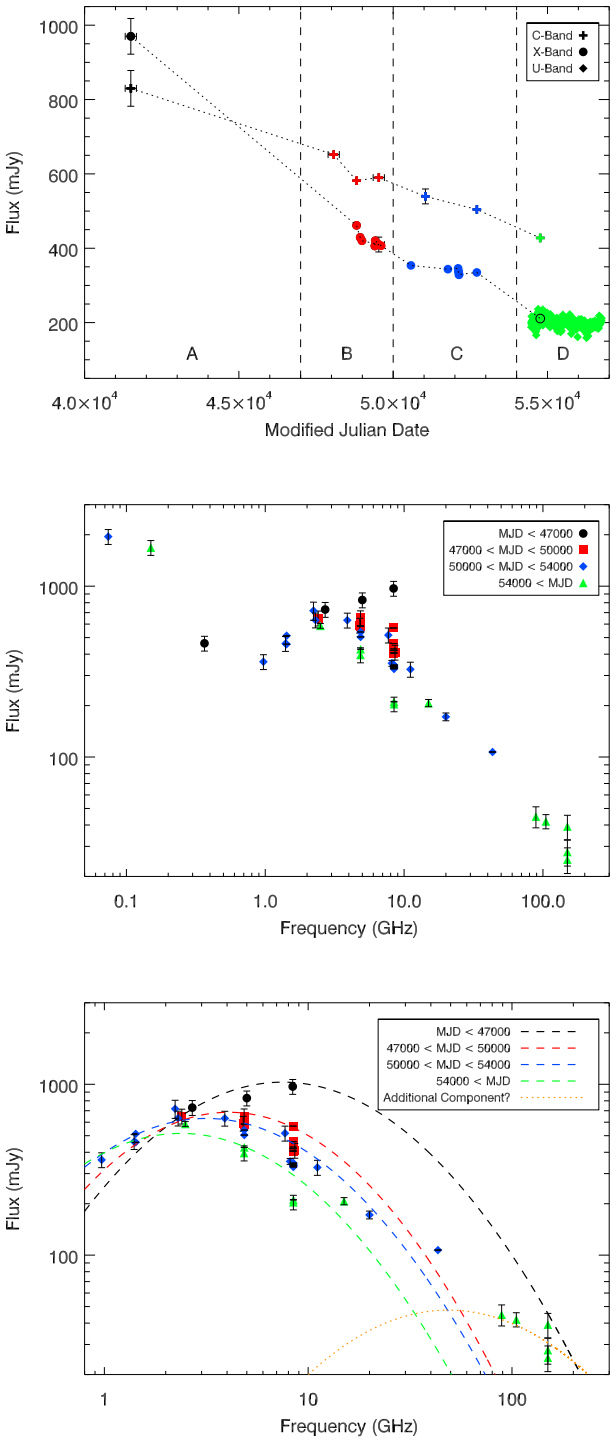

Figure 10. Top panel: *C*- (≈5 GHz), *X*- (≈8 GHz) and *U*-band (≈15 GHz) light curves for RXJ1558-14, showing steady decline since the first data point, in 1972. Note that the *X*-band datum point in time-window D has a border included to differentiate it from the overlapping *U*-band data. Middle panel: SED where points coloured corresponding to the time windows indicated in top-panel. Bottom panel: illustrative fits to the GPS component of the SED for each of the time windows. As time goes on the GPS peak appears to move both downwards and to the lower frequency. Note that the highest frequency points in time-window D (and to a lesser degree window C) appear discrepantly high. This may indicate a new period of activity, illustrated as a dotted orange line in the lower panel. Such indication suggests that a continued VLBI monitoring of this source may see new parsec-scale knots form and propagate outwards within the next few years. [A colour version of this figure is available in the online journal.]

be associated with the launching of individual jet components and may precede the time at which these are observable given current angular resolutions. VLBI monitoring of self-absorbed sources that are varying above a few GHz may therefore allow such flux changes to be directly linked to individual parsec-scale jet components, as has been observed elsewhere (e.g. NGC1275: Suzuki et al. 2012).

The highest frequency data in window D (and a lesser degree, window C) appear discrepantly high and may be indicative of a new period of activity that will become apparent at lower frequencies only as the emitting knots move down-jet and the self-absorption turnover peaks to lower frequency. VLBI monitoring of the source may therefore detect new knots forming and propagating outwards in the coming decade.

In further analogy to NGC1275 we note that RXJ1558-14 has a steep spectrum power-law tail to low frequency. In NGC1275 this tail is associated with a 300 kpc radio mini-halo. A similar structure may be present around RXJ1558-14. However, we note that in the TIFR GMRT Sky Survey imaging of this source there appears to be reasonably symmetric structure extending almost 200 kpc from the core (PA ≈ 91.8) and hence the steep spectrum emission may be indicative of large-scale lobes from a previous large outburst. Interestingly, X-ray cavities are detected by *Chandra* in this source (Hlavacek-Larrondo et al. 2013; Russell et al. 2013) with total physical extent of 17.1 ± 2.3 kpc.

Due to its relatively good long-term SED monitoring we consider RXJ1558-14 as a case study in Fig. 8. We calculate the GPS-peak frequency and measured variability in RXJ1558-14 for each of the four epochs highlighted in Fig. 10. We can directly measure the 15 GHz percentage variability in epoch D only, during which OVRO monitoring data are available. For each of the other three epochs, we measure the *C* band (4.86 GHz) and *X* band (8.44 GHz) values at the epoch boundaries, using these to extrapolate an estimate of the 15 GHz flux. We plot the position of RXJ1558-14 on Fig. 8 during each of these four epochs. Initially, in epoch A we find typically 4 per cent variation annually at 15 GHz. During this epoch the peak is just below 15 GHz and hence the spectrum is still relatively self-absorbed at this frequency. In epoch B we are further in time from the event that caused the peaked component of RXJ1558-14's spectrum. The peak has moved to lower frequency meaning that a steeper part of the spectrum crosses 15 GHz and hence contrary to the general trend we see higher variability during this epoch. In epochs C and D the variability continues to lessen as the turnover frequency drops. It may be possible that a second, sub-dominant component peaked at much higher frequency (see Fig. 10, bottom panel) is also present in the spectrum. If this component varied differently to a lower peaked component then it could show increasing flux as the other was decreasing at 15 GHz and hence could lessen observed monochromatic variability.

5.3 Case study: NGC1275

As presented and discussed in Dutson et al. (2014), NGC1275 has been regularly monitored for over four decades and shows long-term variability both in terms of its GPS-peak frequency and spectral normalization.

In order to place NGC1275 on our Fig. 8 we take estimates of the GPS-peak frequency and 15 GHz variability in three epochs: 1979–83 (epoch a, Fig. 8), 1983–2005 (epoch b) and 2005–2013 (epoch c; see also fig. 5, Abdo et al. 2009). Initially, during epoch a, the peak is well above the 15 GHz monitoring frequency and we see a sharp increase of around 5.5 per cent annually. During epoch b, the self-absorption peak 'rolls up' the spectrum to lower frequency and is

accompanied by a relatively steady decline of about 3 per cent annually over an extended period that may be coinciding with expanding features on parsec scales. Finally in epoch c there is another period of sharply increasing flux (almost 12 per cent per year) which coincides with the peak moving to higher frequencies. Overall the trend is for long-term climbs followed by troughs, with the variability at 15 GHz dependent on both the position of the peak relative to this as well as the underlying variability in the total normalization of the spectrum.

5.4 Comparisons to the general GPS population

An important consideration to make is whether the variability and wide variety of spectral shapes that we are seeing in BCGs, is exclusive only to this special class of objects or whether they are applicable to the wider population of radio sources.

There are many examples of high peaking sources in the literature (e.g. Rodriguez et al. 2014) but large samples are required to fully determine how common these are amongst the overall radio-source population. Classifying peaked radio sources is difficult. Often only non-contemporaneous observations are available meaning that variability of inherently flat spectrum sources can lead them to be misclassified (e.g. see discussion in Tornikoski et al. 2009, and references therein). Alternatively, even when a spectrum is sampled at multiple frequencies and a peak observed, without follow-up over several years it is very difficult to determine whether this is a true, slowly varying GPS source or a usually flat-spectrum source undergoing a rapid flare. Further complicating the issue, it appears as if the contamination of GPS catalogues by variable sources and BL-Lacs is dependent upon the GPS host galaxy; quasar-type GPS sources are much more commonly misidentified than GPS sources in more typical galaxies (Torniainen et al. 2005, 2007).

In the AT20G survey of the southern sky at 20 GHz (Murphy et al. 2010), there are 3763 sources (detection limit of 40 mJy at 20 GHz) that have simultaneous observations at 5, 8 and 20 GHz. Of these, 21 per cent are found to have peaked spectra, 14 per cent show a spectral upturn over this range and 8 per cent are inverted, suggesting a peak above 20 GHz. This fraction of inverted and peaked sources is significantly higher than the $\geq$3.4 per cent of our parent sample peaking above 2 GHz. There is however a clear selection bias towards a higher fraction of inverted and peaked sources in the 20 GHz selected sample than in our sample of BCGs detected at high radio frequencies but selected from a parent sample unbiased by radio priors. Indeed, in the 5 deg^2 sampled down to 2.5 mJy for the AT20g-deep pilot survey (Franzen et al. 2014) 83 sources are detected and have near-simultaneous spectra from 1.4–20 GHz. Of these only 2.4 per cent show a spectral upturn, 15.7 per cent are peaked and 6.0 per cent are peaked above 20 GHz. These reduced fractions of 'exotic' spectral types in comparison to the full AT20G suggest that the area-limited nature of the survey coupled with the deeper detection limit means that more of the 'typical' single-spectrum sources that constitute the bulk of extragalactic radio sources are detected. Franzen et al. (2014) find that about 12 per cent of their sources vary by more than 15 per cent over 3 yr at 20 GHz, which is comparable to the levels of variability we detect for our sources at 15 GHz (see Fig. 8).

Dallacasa et al. (2000) matched 1740 sources with $S_{4.9\,\mathrm{GHz}} > 300$ mJy in the GB6 catalogue (Condon et al. 1994) to the NVSS catalogue (Condon et al. 1998), finding 102 candidate inverted spectra. Simultaneous follow-up of these candidates at 1.365–22.46 GHz with the VLA revealed 55 to be genuinely inverted sources whereas the remaining 47 were flat spectrum sources whose variability meant that non-contemporaneous observations had caused their spectra to appear peaked. These 55 sources (their HFP 'bright sample') thus mean that 3.2 per cent of their initial matched sample have spectral peaks $\geq$3.4 GHz. Taking the same frequency cut we find more than 1.9 per cent of our parent sample peak at similarly high frequencies. Whilst still lower than the detected fraction of Dallacasa et al. (2000), if we consider that our sample contains BCGs detected irrespective of their radio loudness and hence contains a portion of radio-quiet objects then our detection samples are in reasonable agreement. We note that in a follow-up paper, Stanghellini, Dallacasa & Orienti (2009) define an HFP 'faint sample' of sources with $S_{4.9\,\mathrm{GHz}}$ between 50 and 300 mJy in the GB6 sample. 61 HFPs with peaks at frequencies above 1.3 GHz are identified in this sample however they do not state the size of the parent sample, meaning a comparison to their detection fraction cannot be made.

Overall it appears as if the peaked components of our BCG spectra are similar in their properties to the general GPS/HFP populations. However, a worthwhile point to note is that of the 26 sources in which we fit a GPS-like component, 20 of these (representing 76.9 per cent) also contain a steep spectrum power-law to low frequencies. The usual interpretation of peaked radio sources is that they are young (O'Dea 1998). The presence of an accompanying steep component in the majority of our BCGs rules out these being truly young radio sources. Instead, the peaked components could be interpreted as due to either enhanced radio emission at recent times in a long-lived source, or that the radio source in BCGs can be restarted on short time-scales. The low-level variation that we see in our BCGs, coupled with the high duty cycle of detection, points to these being very-long-lived radio sources whose radio output can show quite large variations in magnitude over time. Hancock et al. (2010) followed up 21 sources found to be inverted in the AT20G between 8 and 20 GHz with the Australia Telescope Compact Array at 40 and 95 GHz. Of these 21 targets, 12 were found to be genuine peaked sources, of which 3 (25 per cent) showed evidence of being restarted rather than truly young radio-sources, indicating them to be longer lived sources that have undergone a recent episode of high activity. Although caution must be employed for the small numbers that we are considering, this tentatively supports the idea that peaked components in BCGs are much more commonly attributable to enhanced activity in long-lived sources than in the GPS population as a whole, which is dominated by truly 'young' sources. In other words, BCGs do not just have a single period of strong jet-emitting activity and then fade. They instead live for a long time, but remain active and effectively young at heart.

We point out that continuous radio core activity over a long time is known in galaxies not selected as BCGs; for example, FR II radio sources, which have measured ages of up to 10^8 yr (see e.g. Machalski et al. 2007; Mathews & Guo 2012) – and are *still* being powered – can have cores with radio luminosities similar to those in this paper, with many having flat or rising spectra. However, if the AGN activity of BCGs has been regulating cluster cores for around half the Hubble time (e.g. Vikhlinin 2006; Pratt et al. 2010; McDonald et al. 2014) then this implies activity time-scales over an order of magnitude longer than even these long-lived sources.

5.5 Implications as an SZ contaminant

Considering the SED shapes of our sampled sources (see Appendix A), it is clear that extrapolation of the spectra from below 10 GHz towards the interesting range for SZ decrements

(between roughly 15 and 200 GHz) will in many cases underestimate or completely overlook the contribution of an active self-absorbed component. Added to this is the further complication that variability brings, requiring contemporaneous high-resolution observations to ideally account for contaminants (as is of course possible with interferometric SZ instruments such as AMI and CARMA).

For a sample of 45 galaxy clusters observed at 140 GHz with BOLOCAM, Sayers et al. (2013) used the 1-30 GHz spectral index in addition to limits from their 140 GHz maps to constrain the contamination by point sources. Although they concluded that typically only about 25 per cent of the clusters showed a greater than 1 per cent fractional change of the SZ signal, they noted that this level of contamination was much more prevalent in CC clusters (11/17, roughly 65 per cent). We note that *all* of the BCGs in our current sample are believed to lie in CC clusters. Sayers et al. (2013) detect no clear point sources at 140 GHz from their sample of 17 CCs, whereas from our significantly larger parent sample (40 per cent of our 530 cluster parent sample are tagged as CC: H15a) we detect 32 at 150 GHz. This suggests $\geq$6.0 per cent of BCGs in all clusters exhibit bright BCG emission in the mm-range rising to $\geq$15.1 per cent if only CC clusters are considered. These values are lower limits since our 150 GHz follow-up is flux limited and also incomplete in that some clusters are not observed at 150 GHz. The true level of contamination in CC clusters could therefore be even higher. We note that the prevalence of flattened or inverted spectral components in NCC clusters at frequencies below 20 GHz is much reduced (see H15a); hence the level of contamination at 150 GHz is expected to be significantly lower in these systems.

Interestingly, of the $\geq$15.1 per cent of the CC-hosted BCGs in our sample, more than half ($\geq$8.5 per cent of the total CCs) have a peaked component with a turnover above 2 GHz. Underestimating the point-source contamination will be particularly severe for extrapolation of the lower frequency spectrum in this type of object. SZ catalogues are therefore potentially biased against the inclusion of CC clusters. The true magnitude of line-of-sight integrated Comptonization ($Y_{\rm SZ}$) in these systems may be commonly underestimated, due to BCG radio emission cancelling the SZ decrement. Interestingly this could suggest that the mass bias between X-ray and SZ-derived cluster masses is more prevalent than previously assumed.

During their observations, the Planck Consortium compiled extensive catalogues of high radio-frequency sources (e.g. Planck Collaboration XIII 2011b; Planck Collaboration XXVIII 2014). In Planck Collaboration XIII (2011b) the extragalactic source counts agree with those of the South Pole Telescope (Mocanu et al. 2013), Atacama Cosmology Telescope (Marriage et al. 2011a) and the *Wilkinson Microwave Anisotropy Probe* (Komatsu et al. 2011), at the lower frequency range of *Planck*. However, Planck Collaboration XIII (2011b) show that there may be a steepening of the typical spectral index above 70 GHz which could mean that contamination of the cosmic microwave background (CMB) power spectrum by radio sources below the *Planck* detection limit may be less than currently thought. However, this may only apply to the bright end of the luminosity function. A population of GPS/HFP sources (in addition to a potentially ubiquitous mm/sub-mm component, see Section 5.6) in low-luminosity AGN (LLAGN) and BCGs could present a low-level contaminant to the CMB power spectrum. Deep, high radio-frequency radio surveys are required to shed light on the luminosity function of faint sources in this range.

5.6 Potential additional sub-mm component

Examination of our SEDs (see Section A) shows that a number of sources have inverted spectra between our GISMO observations at 150 GHz and SCUBA-2 observations at 353 GHz. That is, the spectral slope switches from being falling as frequency increases at frequencies below 150 GHz to rising just afterwards. This is most notable in A646, MACS1931-26 and RXJ1504-02. The observed indices are too shallow ($\alpha \approx 1.0$, in all three cases) to be solely attributable to dust emission (expected $\alpha > \approx$2.5; Edge et al. 1999). However, combining the extrapolated flat spectrum core component with the expected dust contribution determined from *Herschel*-SPIRE observations at 250, 350 and 500 μm (Herschel Lensing Survey – HLS; Egami et al. 2010; Rawle et al. 2012) can explain the spectral upturn in MACS1931-26. However, there is still unaccounted for flux of ≈20 and 10 mJy at 353 GHz in A646 and RXJ1504-02, respectively, after accounting for both these contributions, roughly equivalent to P_{353} GHz of 1×10^{24} W Hz^{-1} for both sources.

An intriguing explanation to account for this 'missing flux' is that we may be seeing an additional component in the radio/sub-mm spectrum caused by an advection dominated accretion flow (ADAF: e.g. Mahadevan 1997; Narayan et al. 1998; Ulvested & Ho 2001; Doi et al. 2005; Narayan & McClintock 2008). These are believed to exist, commonly in conjunction with jets, in low radiative efficiency accretion sources. Multiple models exist that aim to explain the bolometric spectra of LLAGN, often invoking a combination ADAF + jet (e.g. Falcke 1996; Wu, Yuan & Cao 2007; Nemmen, Storchi-Bergmann & Eracleous 2014). A common feature of ADAF models is the existence of a synchrotron self-absorbed component that typically peaks at mm-wavelengths. To investigate whether such a component could explain our anomalous SCUBA-2 fluxes we take the base model of Mahadevan (1997) for a black hole mass of 5×10^9 M$_\odot$, with a viscosity parameter of 0.3 and a ratio of gas to total pressure of 0.5. For a typical BCG accretion rate in the ADAF range (e.g. see Russell et al. 2013) of 3×10^{-4}–$3 \times 10^{-5} M_{\rm Edd}$ this predicts an ADAF power of $\sim 1 \times 10^{22-23}$ W Hz^{-1} at 353 GHz. We note that this an order of magnitude lower than would be inferred if all of the missing flux at 353 GHz in A646 and RXJ1504-02 were from an ADAF component. The modelled ADAF-powers scale with black hole mass and accretion rate. However, to align these with our missing flux would require unfeasibly high black hole masses or accretion rates that would no longer be compatible with an ADAF-like accretion structure (e.g. Done, Gierlinski & Kubota 2007). Furthermore, the upturned spectral index is expected to be close to $\alpha \propto 0.4$ for an ADAF (Mahadevan 1997; Anderson, Ulvestad & Ho 2004). Whilst our fitted core components in A646 and RXJ1504-02 underpredict the measured 150 GHz fluxes in both instances (by 1.0 and 0.3 mJy, respectively), a simple interpolation between the 'missing fluxes' at 150 and 353 GHz would give indices far too steep to be attributable to simplest case self-absorption. Alternatively, extrapolation with an index $\propto 0.4$ from the missing flux at 353 GHz would overpredict our measured fluxes at 150 GHz.

For the reasons given above we rule out the presence of a strong ADAF component to explain our missing flux. We note that our findings do not rule out the presence of an ADAF component hidden well below our observed (or missing) flux. The most likely explanation for the 'missing flux' then becomes a combination of low-level dust emission and variability in the jetted core component.

6 CONCLUSIONS

We have expanded the radio SEDs of a sub-sample of 35 BCGs selected from the sample of over 700 clusters considered by H15a. These sources are all hosted by CC clusters where active feedback is believed to occur, and show the brightest flat or inverted components in their spectra at high radio frequencies. These bright cores suggest that the central SMBH is currently accreting at an appreciable rate and so determining the spectra of these cores at higher frequency allows us to investigate possible physical origins for the radio emission. We considered the variability of these sources at both 15 and 150 GHz, enabling us to better understand the amplitudes of variation in SMBHs during their more active phases. We find a wide variety of spectral shapes and in many cases see that these core components exhibit a spectral peak above 2 GHz, similar to the GPS/HFP population of young radio sources. Our results can be summarized as follows.

(i) CC-hosted BCGs contain distinguishable active radio core components in over 60 per cent of cases (H15a). This core can become dominant at frequencies higher than a few GHz. We see in our current sub-sample that $\geq$15.1 per cent of CC-hosted BCGs contain a radio source greater than 3 mJy at 150 GHz (equivalent to a radio power of $\approx 1.2 \times 10^{23}$ W Hz^{-1} at our median redshift of 0.126) and that more than half of these ($\geq$8.5 per cent of all CCs) contain a distinguishable peaked component to their spectra with a turnover frequency above 2 GHz that would be missed by lower frequency observations. This shows that the majority of CC-hosted BCGs show recent activity, of which a significant fraction show strong active accretion at any given time.

(ii) These core components appear to be similar to the GPS/HFP populations that are usually interpreted as young radio sources. That these peaked components are usually accompanied by steeper spectrum power-law emission at lower frequencies suggests that BCGs show near-continuous activity – these sources essentially enjoy a repeated youth.

(iii) Sources do not commonly show strong variability at 15 GHz on short (week to month) time-scales, with a typical limit of $<$10 per cent indicating relatively steady accretion over these time-scales. We note however that there could be variability that we are missing due to it being hidden within error. There is an increased incidence of variation on six-month time-scales at 150 GHz although, accounting for measurement uncertainty, we find that in most cases this variability can only be restricted to an upper limit of $<$35 per cent. That we do see variability on time-scales less than six months at 150 GHz suggests that this emission originates from within a region of less than 0.01 pc, and hence is tracing the inner regions of the jet or accretion flow.

(iv) We find that sources can show steady variation at 15 GHz over 1–5 yr time-scales, although typically with less than 10 per cent per annum. Variability of up to 20 per cent per annum is observed in a small number of sources during the most active periods of their light curves (although we note that our selection of the currently brightest systems may more favourably select highly varying objects).

(v) This year-scale variability is found to be weakly related to the position of the peak in the GPS component of the spectrum. Whilst for any individual source the position of the peak at any given time *does not* serve as a proxy for the definite amount that source will vary, a higher peak *does* indicate an increased likelihood of large-scale fluctuations.

(vi) We find that $\geq$3.4 per cent of BCGs in our parent sample of 530 sources at declinations greater than 30° contain peaked components peaking above 2 GHz.

(vii) The fraction of BCGs with peaked components peaking above 2 GHz increases to $\geq$8.5 per cent if only CC clusters are considered. Overall, we find $\geq$15.1 per cent of CC clusters contain a 150 GHz point source greater than 3 mJy. This suggests that much more than half of all CC clusters with bright 150 GHz central point sources have spectra whereby even well-determined spectral indices below a few GHz would give very large underestimates of the flux at 150 GHz if extrapolated and hence constitute a potential contaminant for SZ surveys as these sources can wipe out any SZ decrements if not fully accounted for.

ACKNOWLEDGEMENTS

We thank the anonymous referee for useful comments and suggestions that have greatly improved this work. MTH acknowledges the support of the Science and Technologies Funding Council (STFC) through studentship number ST/I505656/1. ACE acknowledges support from STFC grant ST/I001573/1. CR acknowledges the support of STFC. ACF and HRR acknowledge support from ERC Advanced Grant Feedback. We wish to thank the staff of the OVRO for allowing us access to data from their monitoring campaign and additional data for the sources they kindly added to the observing schedule. We would also like to thank the observatory staff at the MRAO (AMI), IRAM-30 m (GISMO), CARMA, the JCMT (SCUBA-2) and the GISMO team for their help in preparing and obtaining data. The OVRO 40-m monitoring programme is supported in part by NASA grants NNX08AW31G and NNX11A043G, and NSF grants AST-0808050 and AST-1109911. This research has made use of data from the UMRAO which has been supported by the University of Michigan and by a series of grants from the National Science Foundation, most recently AST-0607523. The James Clerk Maxwell Telescope is operated by the Joint Astronomy Centre on behalf of the Science and Technology Facilities Council of the United Kingdom, the National Research Council of Canada and (until 2013 March 31) the Netherlands Organization for Scientific Research. Additional funds for the construction of SCUBA-2 were provided by the Canada Foundation for Innovation. Support for CARMA construction was derived from the states of California, Illinois and Maryland, the James S. McDonnell Foundation, the Gordon and Betty Moore Foundation, the Kenneth T. and Eileen L. Norris Foundation, the University of Chicago, the Associates of the California Institute of Technology and the National Science Foundation. Ongoing CARMA development and operations are supported by the National Science Foundation under a cooperative agreement, and by the CARMA partner universities. The research leading to the IRAM-30 m results has received funding from the European Commission Seventh Framework Programme (FP/2007-2013) under grant agreement number 283393 (RadioNet3). This research work has used the TIFR GMRT Sky Survey (http://tgss.ncra.tifr.res.in) data products. This research has made use of the NASA/IPAC Extragalactic Database (NED) which is operated by the Jet Propulsion Laboratory, California Institute of Technology, under contract with the National Aeronautics and Space Administration. This research used data from the NRAO archive. The National Radio Astronomy Observatory is a facility of the National Science Foundation operated under cooperative agreement by Associated Universities, Inc.

REFERENCES

Abdo A. A. et al., 2009, ApJ, 699, 31
Akritas M. G., Bershady M. A., 1996, ApJ, 470, 706

Aller H. D., Aller M. F., Latimer G. E., Hodge P. E., 1985, ApJS, 59, 513
Aller M. F., Aller H. D., Hughes P. A., Plotkin R. M., 2002, in Ros E., Porcas R. W., Lobanov A. P., Zensus J. A., eds, Proc. 6th Eur. VLBI Network Symp., New Developments in VLBI Science and Technology. Max-Planck-Institut für Radioastronomie, Bonn, p. 131
Aller M. F., Hughes P. A., Aller H. D., Latimer G. E., Hovatta T., 2014, ApJ, 791, 53
Anderson J., Ulvestad J. S., Ho L. C., 2004, ApJ, 603, 42
Araya E. D., Rodriguez C., Pihlstrom Y., Taylor G. B., Tremblay S., Vermeulen R. C., 2010, AJ, 139, 17
Baars J. W. M., Genzel R., Paulini-Toth I. I. K., Witzel A., 1977, A&A, 61, 99
Barvainis R., Lehar J., Birkinshaw M., Falcke H., Blundell K., 2005, ApJ, 618, 108
Beasley A. J., Gordon D., Peck A. B., Petrov L., MacMillan D. S., Fomalont E. B., Ma C., 2002, ApJS, 141, 13
Benson A. J, Bower R. G., Frenk C. S., Lacey C. G., Baugh C. M., Cole S., 2003, ApJ, 599, 38
Best P., von der Linden A., Kauffmann G., Heckman T. M., Kaiser C. R., 2007, MNRAS, 379, 894
Böhringer H., Voges W., Fabian A. C., Edge A. C., Neumann D. M., 1993, MNRAS, 264, L25
Böhringer H. et al., 2000, ApJS, 129, 435
Böhringer H. et al., 2004, A&A, 425, 367
Bourda G., Charlot P., Porcas R. W., Garrington S. T., 2010, A&A, 520, 113
Bourda G., Collioud A., Charlot P., Porcas R., Garrington S., 2011, A&A, 526, 102
Bower R. G., Benson A. J., Malbon R., Helly J. C., Frenk C. S., Baugh C. M., Cole S., Lacey C. G., 2006, MNRAS, 370, 645
Burns J. O., 1990 AJ 99 14
Burns J. O., Sulkanen M. E., Gisler G. R., Perley R. A., 1992, ApJ, 388, L49
Cavagnolo K. W., Donahue M., Voit M., Sun M., 2008, ApJ, 638, 107
Chapin E. L., Berry D. S., Gibb A. G., Jenness T., Scott D., Tilanus R. P. J., Economou F., Holland W. S., 2013, MNRAS, 430, 2545
Coble K. et al., 2007, AJ, 134, 897
Cohen A. S., Lane W. M., Cotton W. D., Kassim N. E., Lazio T. J. W., Perley R. A., Condon J. J., Erickson W. C., 2007, AJ, 134, 1245
Condon J. J., Broderick J. J., Seielstad G. A., Douglas K., Gregory P. C., 1994, AJ, 107, 1829
Condon J. J., Cotton W. D., Greisen E. W., Yin Q. F., Perley R. A., Taylor G. B., Broderick J. J., 1998, ApJ, 115, 1693
Conselice C. J., Gallagher J. S., III, Wyse R. F. G., 2001, AJ, 122, 2281
Crawford C. S., Allen S. W., Ebeling H., Edge A. C., Fabian A. C., 1999, MNRAS, 306, 857
Croton D. J. et al., 2006, MNRAS, 365, 11
Dallacasa D., Stanghellini C., Centonza M., Fanti R., 2000, A&A, 363, 887
De Breuck C., Tang Y., de Bruyn A. G., Röttgering H., van Breugel W., 2002, A&A, 394, 59
Doi A., Kameno S., Kohno K., Nakanishi K., Inoue M., 2005, MNRAS, 363, 692
Done C., Gierlinski M., Kubota A., 2007, A&AR, 15, 1
Douglas J. N., Bash F. N., Bozyan F. A., Torrence G. W., Wolfe C., 1996, AJ, 111, 1945
Dunn R. J. H. Fabian A. C., 2008, MNRAS, 385, 757
Dutson K. L., Edge A. C., Hinton J. A., Hogan M. T., Gurwell M. A., Alston W. N., 2014, MNRAS, 442, 2048
Ebeling H., Edge A. C., Böhringer H., Allen S. W., Crawford C. S., Fabian A. C., Voges W., Huchra J. P., 1998, MNRAS, 301, 881
Ebeling H., Edge A. C., Allen S. W., Crawford C. S., Fabian A. C., Huchra J. P., 2000, MNRAS, 318, 333
Edge A. C., 2001, MNRAS, 328, 762
Edge A. C., Ivison R. J., Smail I., Blain A. W., Kneib J.-P., 1999, MNRAS, 306, 599
Egami E. et al., 2010, A&A, 518, L12
Ehlert S. et al., 2011, MNRAS, 411, 1641
Fabian A. C., 1994, ARA&A, 32, 277
Fabian A. C., 2012, ARA&A, 50, 455
Fabian A. C. et al., 2000, MNRAS, 318, 65
Fabian A. C., Reynolds C. S., Taylor G. B. Dunn R. J. H., 2005, MNRAS, 363, 891
Falcke H., 1996, ApJ, 464, L67
Fey A. L., Charlot P., 2000, ApJS, 128, 17
Franzen T. M. O. et al., 2011, MNRAS, 415, 2699
Franzen T. M. O. et al., 2014, MNRAS, 439, 1212
Giacintucci S., Markevitch M., Brunetti G., Cassano R., Venturi T., 2011, A&A, 525, L10
Gioia I. M. Henry J. P., Mullis C. R., Böhringer H., Briel U. G., Voges W., Huchra J. P., 2003, ApJS, 149, 29
Gitti M., Ferrari C., Domainko W., Feretti L., Schindler S., 2007, A&A, 470, L25
Gooch R. E., 1996, in Jacoby G. H., Barnes J., eds, ASP Conf. Ser. Vol. 101, Astronomical Data Analysis Software and Systems V. Astron. Soc. Pac., San Francisco, p. 80
Gregory P. C., Condon J. J., 1991, ApJS, 75, 1011
Hales S. E. G., Riley J. M., Waldram E. M., Warner P. J., Baldwin J. E., 2007, MNRAS, 382, 1639
Hamer S. L. et al., 2014, MNRAS, 437, 862
Hancock P. J., Sadler E. M., Mahony E. K., Ricci R., 2010, MNRAS, 408, 1187
Hasselfield M. et al., 2013, J. Cosmol. Astropart. Phys., 07, 008
Healey S. E., Romani R. W., Taylor G. B., Sadler E. M., Ricci R., Murphy T., Ulvestad J. S., Winn J. N., 2007, ApJS, 171, 61
Helmboldt J. F. et al., 2007, ApJ, 658, 203
Hlavacek-Larrondo J., Fabian A. C., Edge A. C., Ebeling H., Sanders J. S., Hogan M. T., Taylor G. B., 2012, MNRAS, 421, 1360
Hlavacek-Larrondo J., Fabian A. C., Edge A. C., Ebeling H., Allen S. W., Sanders J. S., Taylor G. B., 2013, MNRAS, 431, 1638
Hogan M. T. et al., 2015, MNRAS, 453, 1201
Holland W. S. et al., 2013, MNRAS, 430, 2513
Hopkins P. F., 2012, MNRAS, 420, L8
Hovatta T., Tornikoski M., Lainela M., Lehto H. J., Valtaoja E., Torniainen I., Aller M. F., Aller H. D., 2007, A&A, 469, 899
Iwasawa K., Allen S. W., Fabian A. C., Edge A. C., Ettori S., 1999, MNRAS, 306, 467
Jenness T., Berry D., Chapin E., Economou F., Gibb A., Scott D., 2011, in Evans I. N., Accomazzi A., Mink D. J., Rots A. H., eds, ASP Conf. Ser. Vol. 442, Astronomical Data Analysis Software and Systems XX. Astron. Soc. Pac., San Francisco, p. 281
Kempner J. C., Blanton E. L., Clarke T. E., Enßlin T. A., Johnston-Hollitt M., Rudnick L., 2004, in Kempner R. J., Soker N., eds, The Riddle of Cooling Flows in Galaxies and Clusters of Galaxies, p. 335, available at http://www.astro.virginia.edu/coolflow/proc.php
Knox L., Holder G. P., Church S. E., 2004, ApJ, 612, 96
Knudsen K. K., van der Werf P. P., Kneib J.-P., 2008, MNRAS, 384, 1611
Komatsu E. et al., 2011, ApJS, 192, 18
Kovács A., 2008, in Duncan W. D., Holland W. S., Withington S., Zmuidzinas J., eds, Proc. SPIE Conf. Ser. Vol. 7020, Millimeter and Submillimeter Detectors and Instrumentation for Astronomy IV. SPIE, Bellingham, p. 70201s
Krichbaum T. P. et al., 1992, A&A, 260, 33
Lane W. M., Cotton W. D., van Velzen S., Clarke T. E., Kassim N. E., Helmboldt J. F., Lazio T. J. W., Cohen A. S., 2014, MNRAS, 440, 327
Laurent-Muehleisen S. A., Kollgaard R. I., Ryan P. J., Feigelson E. D., Brinkmann W., Siebert J., 1997, A&AS, 122, 235
Lin Y., Partridge B., Pober J. C., Bouchefry K. E., Burke S., Klein J. N., Coish J. W., Huffenberger K. M., 2009, ApJ, 694, 992
Liuzzo E., Giovannini G., Giroletti M., 2009, in Heinz S., Wilcots E., eds, AIP Conf. Proc. Vol. 1201, The Monsters Fiery Breath: Feedback in Galaxies, Groups, and Clusters. Am. Inst. Phys., New York, p. 186
McDonald M. et al., 2014, ApJ, 794, 67
Machalski J., Chyzy K. T., Stawarz Ł., Kozieł D., 2007, A&A, 462, 43
Mcnamara B. R., Nulsen P. E. J., 2007, ARA&A, 45, 117
Mcnamara B. R., Nulsen P. E. J., 2012, New J. Phys., 14, 055023
McNamara B. R. et al., 2000, ApJ, 534, L135

Magorrian J. et al., 1998, AJ, 115, 2285
Mahadevan R., 1997, ApJ, 477, 585
Marriage T. A. et al., 2011a, ApJ, 731, 100
Marriage T. A. et al., 2011b, ApJ, 737, 61
Massardi M., Ekers R. D., Murphy T., Mahony E., Hancock P. J., Chhetri R., 2011, MNRAS, 412, 318
Massaro E., Giommi P., Leto C., Marchegiani P., Maselli A., Perri M., Piranomonte S., Sclavi S., 2009, A&A, 495, 691
Mathews W. G., Guo F., 2012, ApJ, 755, 13
Mauch T., Murphy T., Buttery H. J., Curran J., Hunstead R. W., Piestrzynska B., Robertson J. G., Sadler E. M., 2003, MNRAS, 342, 1117
Merloni A., Heinz S., di Matteo T., 2003, MNRAS, 345, 1057
Merloni A., Rudnick G., Di Matteo T., 2004, MNRAS, 354, L37
Mittal R., Hudson D. S., Reiprich T. H., Clarke T., 2009, A&A, 501, 835
Mocanu L. M. et al., 2013, ApJ, 779, 61
Murphy T. et al., 2010, MNRAS, 402, 2403
Nagai H. et al., 2010, PASJ, 62, L11
Narayan R., McClintock J. E., 2008, New Astron. Rev., 51, 733
Narayan R., Mahadevan R., Grindlay J. E., Popham R. G., Gammie C., 1998, ApJ, 492, 554
Nemmen R. S. S., Storchi-Bergmann T., Eracleous M., 2014, MNRAS, 438, 2804
Nulsen P. E. J., McNamara B. R., 2013, Astron. Nachr., 334, 386
O'Dea C. P., 1998, PASP, 110, 493
O'Dea C. P. et al., 2008, ApJ, 681, 1035
Orienti M., Dallacasa D., 2014, MNRAS, 438, 463
Pauliny-Toth I. I. K., Kellermann K. I., 1966, ApJ, 146, 634
Perlman E. S., Schachter J. F., Stocke J. T., 1999, Am. Astron. Soc. Meeting, 195, 1601
Peterson J. R., Kahn S. M., Paerels F. B. S., Kaastra J. S., Tamura T., Bleeker J. A. M., Ferrigno C., Jernigan J. G., 2003, ApJ, 590, 207
Petrov L., 2011, AJ, 142, 105
Pfrommer C., Enßlin T. A., 2003, A&A, 407, L73
Planck Collaboration VII, 2013, A&A, 550, A133
Planck Collaboration VIII, 2011, A&A, 536, A8
Planck Collaboration XIII, 2011, A&A, 536, A13
Planck Collaboration XXVIII, 2014, A&A, 571, A28
Planck Collaboration XXIX, 2014, A&A, 571, A29
Pratt G. W. et al., 2010, A&A, 511, A85
Rafferty D. A., McNamara B. R., Nulsen P. E. J., 2008, ApJ, 687, 899
Randall S. W. et al., 2011, ApJ, 726, 86
Rawle T. D. et al., 2012, ApJ, 747, 29
Reichardt C. L. et al., 2013, ApJ, 763, 127
Rengelink R. B., Tang Y., de Bruyn A. G., Miley G. K., Bremer M. N., Roettgering H. J. A., Bremer M. A. R., 1997, A&AS, 124, 259
Richards J. L. et al., 2011, ApJS, 194, 29
Rodriguez L. F., Carrasco-Gonzalez C., Montes G., Tapia M., 2014, AJ, 148, 20
Russell H. R., Fabian A. C., Sanders J. S., Johnstone R. M., Blundell K. M., Brandt W. N., Crawford C. S., 2010, MNRAS, 402, 1561
Russell H. R., McNamara B. R., Edge A. C., Hogan M. T., Main R. A., Vantyghem A. N., 2013, MNRAS, 432, 530
Sadler E. M. et al., 2006, MNRAS, 371, 898
Salome P., Combes F., 2003, A&A, 412, 6574
Sanderson A. J. R., Edge A. C., Smith G. J., 2009, MNRAS, 398, 1698
Sayers J. et al., 2013, ApJ, 764, 152
Shabala S., Alexander P., 2007, Ap&SS, 311, 311
Silk J., Rees M. J., 1998, A&A, 331, L1
Smail I., Ivison R. J., Blain A. W., Kneib J.-P., 2002, MNRAS, 331, 495
Springel V., Di Matteo T., Hernquist L., 2005, MNRAS, 361, 776
Staguhn J. et al., 2008, J. Low Temp. Phys., 151, 709
Stanghellini C., Dallacasa D., Orienti M., 2009, Astron. Nachr., 330, 223
Sunyaev R. A., Zel'dovich Y. B., 1972, Comments Astrophys. Space Phys., 4, 173
Suzuki K. et al., 2012, ApJ, 746, 140
Taylor G. B., 1996, ApJ, 470, 394
Torniainen I., Tornikoski M., Teräsranta H., Aller M. F., Aller H. D., 2005, A&A, 435, 839
Torniainen I., Tornikoski M., Lähteenmäki A., Aller M. F., Aller H. D., Mingaliev M. G., 2007, A&A, 469, 451
Tornikoski M., Torniainen I., Lähteenmäki A., Hovatta T., Nieppola E., Turunen M., 2009, Astron. Nachr., 330, 128
Ulvestad J. S., Ho L. C., 2001, ApJ, 562, L133
Vanderlinde K. et al., 2010, ApJ, 722, 1180
Vikhlinin A., 2006, ApJ, 640, 710
White R. L., Becker R. H., Helfand D. J., Gregg M. D., 1997, ApJ, 475, 479
Woody D. P. et al., 2004, in Zmuidzinas J., Holland W. S., Withington S., eds, Proc. SPIE Conf. Ser. Vol. 5498, Millimeter and Submillimeter Detectors for Astronomy II. SPIE, Bellingham, p. 30
Wootten A., Thompson A. R., 2009, Proc. IEEE, 97, 1463
Wright A., Otrupcek R., 1990, PKS Catalog
Wu Q., Yuan F., Cao X., 2007, ApJ, 669, 96
Yi I., Boughn S. P., 1998, ApJ, 499, 198
Zemcov M., Borys C., Halpern M., Mauskopf P., Scott D., 2007, MNRAS, 376, 1073
Zwart J. T. L. et al., 2008, MNRAS, 391, 1545

SUPPORTING INFORMATION

Additional Supporting Information may be found in the online version of this article:

Table 2. GISMO (150 GHz) fluxes of the observed clusters.
Table 3. AMI (16 GHz) fluxes of the observed BCGs.
Table 4. CARMA (90 GHz) fluxes of the observed BCGs.
Table 5. SCUBA-2 (353 GHz) fluxes of the observed BCGs.
Figure A1. SEDs for sources within our sample.
Figure A2. SEDs, continuation of Fig. A1.
Figure A3. SEDs, continuation of Fig. A1.
Figure A4. SEDs, continuation of Fig. A1.
Figure A5. SEDs, continuation of Fig. A1.
Figure A6. SEDs, continuation of Fig. A1.
(http://mnras.oxfordjournals.org/lookup/suppl/doi:10.1093/mnras/stv1518/-/DC1).

Please note: Oxford University Press is not responsible for the content or functionality of any supporting materials supplied by the authors. Any queries (other than missing material) should be directed to the corresponding author for the paper.

This paper has been typeset from a TEX/LATEX file prepared by the author.